USING OBSERVATIONS AND MODEL SIMULATIONS TO CHARACTERIZE THE EFFECTS OF LATERAL INTRUSION EVENTS IN BEDFORD BASIN

by

Edmundo David Garcia Larez

Submitted in partial fulfilment of the requirements
for the degree of Master of Science

at

Dalhousie University
Halifax, Nova Scotia
November 2023

TABLE OF CONTENTS

LIST OF FIGURES

ABSTRACT

The renewal of deep water in Bedford Basin (BB) is vital for its ventilation. The main ventilation mechanisms are winter convention and lateral intrusion events. However, a characterization of intrusion events has not yet been undertaken. Due to global warming, it is expected that the reliability of winter convection events as a ventilation mechanism will decrease. Therefore, a better understanding of the effects of intrusion events is imperative since they may assume greater importance for the ventilation of BB in the future. The main objective of this thesis is to characterize the frequency and effects of intrusion events into BB using both observational data from the Bedford Basin Monitoring Program (BBMP) and two 20-year multi-nested model simulations of BB (HRM2 and HRM23). Where HRM2 is a one-way nesting simulation (low spatial resolution) and HRM23 is a two-way nesting simulation (high spatial resolution). Based on the BBMP dataset, these events cause sharp decreases in nitrate and sharp increases in temperature, salinity, and oxygen. They can occur from spring to fall. However, the majority and the most impactful intrusions occur later in the year. Fall intrusions cause larger disturbances than summer/spring intrusions in the variables mentioned previously and have a larger impact on the stratification of the water column. Overall, HRM23 outperforms HRM2 since it more closely resembles the observed trends in the BBMP dataset. The reliability of weekly and daily data acquisition for identifying intrusion events was evaluated and compared using HRM23. The results indicate that weekly sampling is sufficient for intrusion identification, but for characterizing the effect of these intrusions daily data would be preferrable. The intrusions were also categorized based on their extent along the Basin. This highlighted the presence of intrusions that do not make it to the bottom of BB and therefore are not recorded by the BBMP sampling. In addition, the speed at which these intrusions approach the Basin increased from January to December. Future work should be focused on a more quantitative study of the effects of mixing regimes observed after and during intrusion events, and on performing a similar study with the biological component of the model.

LIST OF ABBREVIATIONS AND SYMBOLS

Abbreviation	Definition
BB	Bedford Basin
BBMP	Bedford Basin Monitoring Program
ROMS	Regional Ocean Modelling System
HRM	Halifax Regional Municipality
BIO	Bedford Institute of Oceanography
GLORYS	Global Ocean Reanalysis
ACM	Atlantic Canada Model
GEBCO	General Bathymetry Chart of the Ocean
HRM1	Model simulation of the Central Scotian Shelf (One-way nesting)
HRM2	Model simulation of the Inner Scotian Shelf (One-way nesting)
HRM3	Model simulation of BB and the Narrows (One-way nesting)
HRM23	Model simulation of BB and the Narrows (Two-way nesting)
NONNA	Canadian hydrographic services for non-navigational purposes bathymetry
NARR	North American Regional Analysis
SS	Intrusion events occurring during spring and summer
OI_{missed}	Number of manually identified intrusions that were missed by the algorithm
OI_{all}	Total number of manually identified intrusion events
AI_{only}	Number of intrusion events only identified by the algorithm
AI_{all}	Total number of intrusion events identified by the algorithm
Δv_{day}	The change in variable (v) per day flagged by the algorithm as an event
$min\Delta v_{day}$	Minimum change in v per day allowed to be part of the flagged event's 'tails'

ACKNOWLEDGEMENTS

I would like to express my deepest gratitude to my supervisor, Dr. Katja Fennel, for their support and guidance throughout the course of my research. Your expertise and patience have greatly contributed to my professional, academic, and personal growth. I am extremely grateful to the faculty and staff at the Department of Oceanography at Dalhousie University. In particular, I would like to thank Dr. Arnaud Laurent and Dr. Bin Wang, who have provided me with essential guidance and encouragement throughout this journey. Also, I would like to give my appreciation to my committee members Dr. Arnaud Laurent, Dr. Will Burt, Dr. Christopher Algar, and Dr. Jinyu Sheng for their insightful comments and advice. As well as to my external Dr. Ruth Musgrave for taking the time to read the thesis and provide feedback. Special thanks to Dr. Christopher Algar, Dr. Ruth Musgrave, and Dr. Stephanie Kienast for giving me the opportunity to perform fieldwork in the Bedford Basin and fulfill the sea time requirement of the program. My sincere thanks also go to the team at the Bedford Institute of Oceanography and MEOPAR for making the Bedford Basin Monitoring Program (BBMP) dataset accessible. To my peers in the master's program, you have made this journey memorable. I am particularly grateful to Haley Geizer, who has provided consistent support, constructive criticism, and much-needed breaks from our work. I would also like to acknowledge the financial support received from Dr. Katja Fennel. Without this support, this research would not have been possible. Lastly, but by no means least, I would like to thank my family. To my mom and dad, your unwavering belief in my abilities and your constant encouragement has helped me through difficult moments throughout my studies. Completing this thesis has been a challenging but rewarding endeavour, and I am grateful to each individual who contributed to this process in some way.

CHAPTER 1

INTRODUCTION

1.1 Background and Significance

Bedford Basin is an estuary that forms part of Halifax Harbour on the Atlantic coast of Nova Scotia, Canada (Figure 1.1). It is a complex and dynamic system where physical, biological, and chemical processes interact to determine water circulation and properties. One geographical characteristic of the Basin that heavily controls its seasonal oceanographic properties is the presence of a relatively shallow channel called the Narrows, that connects BB and the Scotian Shelf. While this channel allows for the interaction of surface water between the Basin and the ocean, it also isolates the bottom waters of BB. This isolation becomes more evident during summer when strong stratification separates the surface and bottom water circulation (Haas et al., 2022). These factors put the bottom waters of the BB especially at risk of developing hypoxic conditions (Fennel and Testa, 2019). Deep water renewal events lead to the redistribution and/or addition of oxygen to the water column, and consequently, they can modify the oxygen concentrations at the bottom of the Basin. The two major renewal mechanisms in BB are density instabilities that cause parcels of water to travel from the surface to different depths of the water column (e.g., winter convection), and fast-moving lateral intrusions of dense offshore water masses that interact with the bottom waters of the Basin (Platt et al., 1972). Understanding these processes is vital for predicting and managing the impacts of environmental changes that may stress the dynamic equilibrium of this ecosystem in the future.

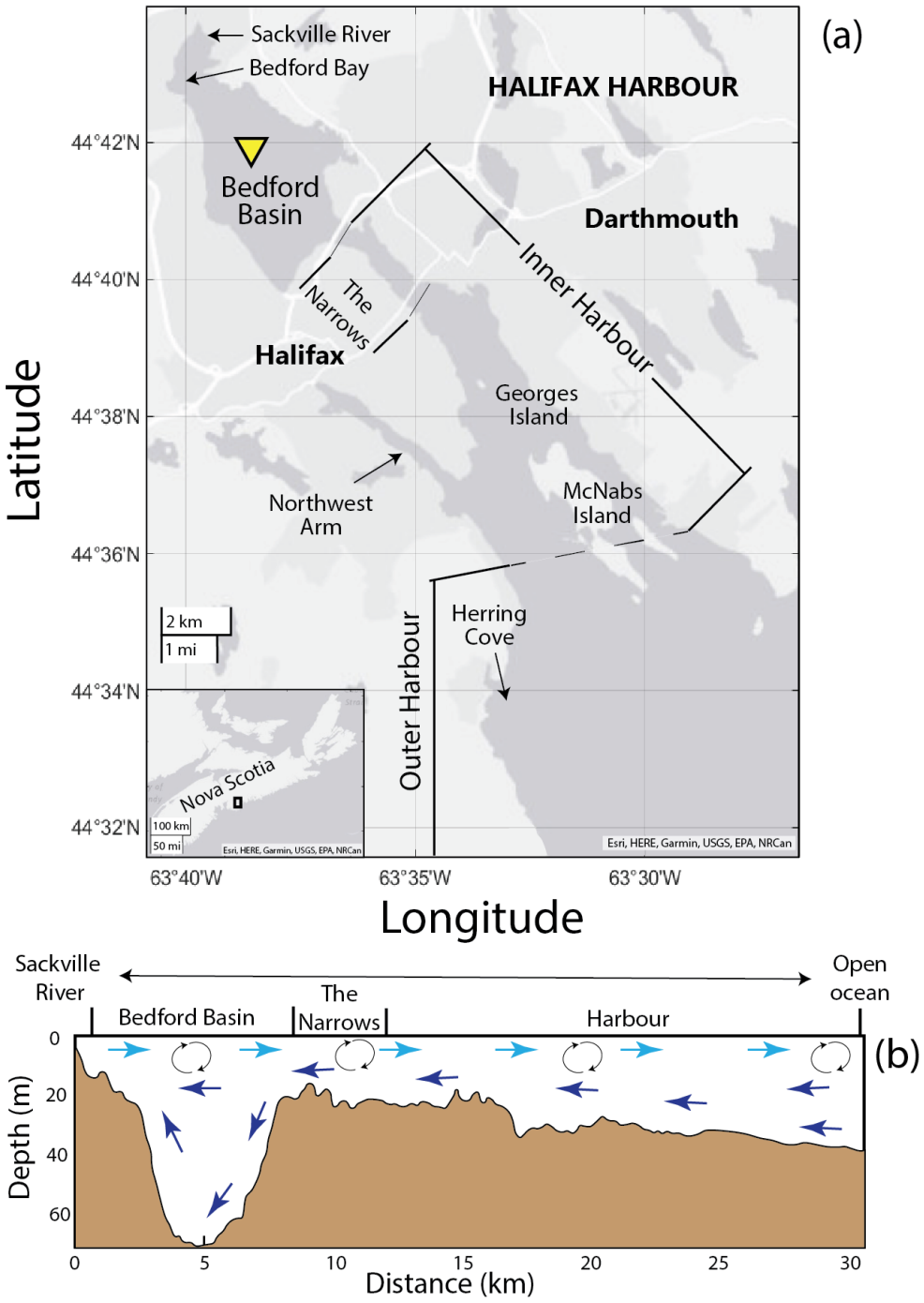

Figure 1.1. (a) Map of the Halifax Harbour in Halifax, NS. The yellow symbol marks the location of the BBMP station**. (b)** Schematic of a cross-section of the Halifax Harbour from the Sackville River to the open ocean.

The annual balance between respiration and oxygen renewal of the bottom waters determines the likelihood of hypoxic conditions developing between winter convection events in BB. The strong stratification in the upper column that develops during late spring is terminated when winter convection events homogenize the water column (Shan et al., 2011). These events contribute to the majority of the bottom water ventilation that occurs in the Basin (Rakshit et al., 2023). Since winter convection events affect the entire water column; they also dictate the amount of oxygen available in the bottom waters until the next winter convection event occurs. However, intrusion events can occur before these winter convection events and can cause deep water renewal earlier during the year by interrupting the isolation and introducing oxygen-rich water masses. In other words, these events prevent the bottom layer from developing anoxic conditions (Hargrave et al., 1976) by acting as a supply of oxygen to the Basin between convection events. Both lateral intrusion events and winter convection play a vital role in shaping the seasonal oxygen patterns observed in the bottom waters of BB. However, it is expected that temperature increases due to climate change could affect the frequency and intensity of winter convection by decreasing the water heat loss to the atmosphere (Rakshit et al., 2023; see Appendix A). This would result in a decrease in the intensity of convection events and consequently affect their reliability as bottom water ventilation mechanisms. Therefore, it is essential to characterize the frequency and effects of lateral intrusion events since they may assume greater importance in the future.

1.2 Definition of lateral intrusion events

In addition to the above-mentioned oxygen renewal generated by winter convection, instances of strong intrusion events in BB were documented in the literature. These include, but are not limited to, one in 2002 (Punshon and Moore, 2004), one in 2010 (Burt et al., 2013), five from 2014 to 2017 (Haas et al., 2021), and two in 2018 (Rakshit et al., 2023). The adjective ‘strong’ is used to describe the rate at which the effects of the intrusions are observed. Slow water intrusions into BB from the outer harbour, or weak intrusions, are a common occurrence due to the two-layer estuarine circulation characteristic of the area. Therefore, strong intrusion events are a subset of intrusions that substantially change the composition of the local water

over a short period of time. These events replace the pre-existing water by introducing water masses with relatively lower concentrations of nitrate, and relatively higher temperature, salinity, and oxygen concentrations than the surrounding waters (Burt et al., 2018; Haas et al., 2021; Haas et al., 2022, Rakshit et al., 2023). The mechanism for strong intrusion events was described by Platt et al. (1972) as a combined effect of intense alongshore winds and tides that causes dense water masses from the Scotian Shelf to intrude into BB. More specifically, the alongshore wind in the Northern Hemisphere drives Ekman transport in the offshore direction. Consequently, this causes wind-driven upwelling and potentially strong lateral intrusion events in BB. The predominant wind direction in the area is southerly/southwesterly in the summer, and westerly/northwesterly in the winter (Environmental Assessment Report, 2013). While intrusions have been identified from summer to fall, the majority of these events occur during fall, perhaps indicating that the mechanism for strong intrusion is more effective during these months. Moreover, these water masses are denser than the surrounding water, and therefore the effects are commonly observed in the deepest sections of BB. However, strong intrusions have also been observed at mid-depth (Shi and Wallace, 2018). In this thesis, the focus will be on strong deep water intrusion events, and any mention of intrusions specifically pertains to this subset of lateral intrusions unless stated otherwise.

1.3 Research Objectives

The Bedford Basin Monitoring Program (BBMP) is a major source of oceanographic observations in BB. Since 1992 the BBMP has recorded weekly profile data at the centre of the Basin. The observations obtained from this data acquisition framework were utilized for multiple research studies including biogeochemical (La Roche, 1983; Azetsu-Scott and Johnson, 1994; Robicheau et al., 2022), geological (Buckley and Winters, 1992; Miller et al., 1982), environmental (Pan and Subba Rao, 1997; Lacasse at al., 2013), model developing (Shan et al. 2011), and other aspects of BB. This includes studies that mentioned the occurrence of strong intrusion events. Currently, the BBMP dataset from 1999 to the present can be used to further our understanding of these events and their possible effects on BB. However, this dataset comes with some limitations regarding the identification of intrusion events. The first limitation is the lack

of horizontal resolution. Since the location of the monitoring station is in the middle of the Basin, limited information is available from other locations within BB. The second limitation is that the station is located ~ 3 km from the Narrows (Figure 1.1). Therefore, any strong lateral intrusion that does not reach the BBMP station will not be recorded in the BBMP dataset. Lastly, the frequency of the data acquisition at the station might be too coarse to identify all the events since they can occur in timescales of hours (Rakshit et al., 2023). Therefore, a weekly sampling might not be enough to study these events properly. Due to all these limitations, it is unrealistic that this dataset alone would provide enough information to comprehensively characterize the frequency and effects of intrusion events.

A realistic numerical simulation is useful given the aforementioned limitations and is used here to complement the observations. Several numerical models of different complexities have been developed for Halifax Harbour including, but not limited to, a simple box model used by Petrie and Yeats (1990) which demonstrated the two-layer estuarine-type circulation of the Basin. A two-dimensional (2D) hydrodynamic model was developed by Tee and Petri (1991) and used to highlight the role of freshwater discharge as the primary driver of the estuarine circulation present in the Harbour. A three-dimensional (3D) linear harmonic finite element model used to simulate the M_2 tides in the Harbour was developed by Greenberg et al. (1999). These are only a few of the models that have been developed for Halifax Harbour to investigate and explain different phenomena. For this thesis, I used the simulations from a model based on the Regional Ocean Modelling System (ROMS) that is based on earlier work by Sui (2023). Nevertheless, it is important to remember that model simulations are subject to inherent limitations, and thus, their results should not be regarded as absolute truth but rather as estimations. By comparing the simulated and the observed strong intrusions, the model's performance can be assessed, and the results can contribute to its further development. The main objectives of this thesis are:

1. To assess the frequency and the effects of strong intrusion events into BB, employing a combination of observational data and model simulations.

2. To evaluate the ability of a numerical ocean circulation model of BB at simulating strong intrusion events.
3. To assess the reliability of the current data acquisition strategy from the BBMP in identifying strong intrusion events by using the flexibility of the model simulation to experiment with different time resolutions and different locations within the BB.

1.4 Thesis Structure

Chapter 2 provides an overview of BB, a characterization of the deep intrusion events observed in the BBMP dataset, and a comparison between the events present in the observations and model results. In Chapter 3, a methodology was developed to systematically identify intrusion events. This methodology was used to compare the intrusion identification skills of a daily and a weekly data acquisition framework at the BBMP station. In addition, in Chapter 3, more data acquisition stations were added to the model simulation to evaluate the reliability of the location of the BBMP station in identifying all the intrusion events affecting BB. Comparisons between simulated intrusions and observed intrusions are also discussed in Chapter 3. And lastly, in Chapter 4, I summarize and discuss my findings.

CHAPTER 2

CHARACTERIZATION AND COMPARISON OF INTRUSION EVENTS FROM OBSERVATIONAL STUDIES AND MODEL SIMULATIONS AT THE BBMP

This chapter describes the methods employed to characterize intrusions of water masses into BB at the BBMP station, provides examples and the results of this characterization for both observations and model results and quantitatively and qualitatively compares both datasets. It provides relevant information about the study site, including seasonal patterns, the design of the observational study and the model simulations, providing justifications for the methodological choices made.

2.1 Study Area

Bedford Basin is an 8-km long fjord with an approximated area of 17 km^2 and a maximum depth of 71 m located in the Halifax Regional Municipality (HRM), Nova Scotia. The Basin is part of the Halifax Harbour which also includes geographic areas such as the Northwest Arm, the Narrows, and the inner and outer harbour (Figure 1.1a). Interactions between BB and Scotian Shelf are constricted by the Narrows, a 300-m-wide and 20-m-deep channel (Li and Harrison, 2008; Petri and Yeats, 1990), which to some degree isolates the Basin. Climate normals calculated from 1981 to 2010 at the Halifax Citadel range from - 0.1 to - 8.2 ºC in January and 23.1 to 15.1 ºC in August (source: Environment and Climate Change Canada; https://climate.weather.gc.ca/climate_normals/results_1981_2010_e.html?searchType=stnProv&lstProvince=NS&txtCentralLatMin=0&txtCentralLatSec=0&txtCentralLongMin=0&txtCentralLongSec=0&stnID=6358&dispBack=0, last access: January 2023). The circulation of BB is characterized as a two-layer, estuarine-type circulation (Figure 1.1b; Huntsman, 1924). The circulation is primarily driven by the discharge of freshwater from the Sackville River and to a lesser extent the saltier return flow from the outer

harbour (Fader and Miller, 2008). Other freshwater inputs to the Basin include wastewater outflow and other smaller watercourses in the area. In terms of volume, the water contributions of freshwater from the Sackville River are small in comparison to the contributions of more saline waters from the Scotian Shelf into the Basin. Nevertheless, as mentioned before, the energy from the riverine input is the main driver of the circulation in BB. The ratio between the tidal inflow and the input of freshwater into the BB is ~100 (Gregory et al., 1993). This causes the salinity in the BB to be lower than that of the Scotian Shelf by ~1 (Kerrigan et al., 2017). Average annual inputs of freshwater into BB were estimated by Buckley and Winters (1992) to be 15.68 m^3 s^{-1}, where ~84% comes from fluvial sources and ~16% from sewage. Of the total amount, ~34% comes from the Sackville River and the next largest source of fluvial fresh water comes from the Paper Mill Lake flume with ~8%. Discharge from the Sackville River reaches its maximum during spring with values of ~9 m^3 s^{-1} and it steadily decreases to ~2 m^3 s^{-1} by the end of summer (Fournier, 1990). The Halifax Harbour experiences semi-diurnal tidal elevations with a mean tidal range of ~1.3 m (Lawrence, 1989). Contributions from the outer harbour to the BB are introduced through the Narrows with an M_2 current magnitude of ~0.23 m s^{-1} (McGonigal et al. 1974).

2.1.1 Seasonal Patterns of physical oceanographic conditions in BB

Temperature and salinity climatological means from 2000 to 2015 in BB were obtained from the BBMP (source: Bedford Institute of Oceanography; https://www.bio.gc.ca/science/monitoring-monitorage/bbmp-pobb/bbmp-pobb-en.php, last access: January 2023). BB experiences strong seasonal variations in water temperature in the top 30 m (Li et al. 2010), corresponding to a delayed reaction from seasonal variations in heat flux. Climatological averages at 10 m depth show temperatures ranging from ~2 ºC in February to <13 ºC in September, and salinity ranging from >30 in November and December to < 31 in July. Moreover, at 60 m, temperatures range from >1.5 ºC in April to <5 ºC in January, and salinity ranges from ~31 in March to <31.5 in December and January. While the mixed-layer temperatures vary seasonally, average yearly temperatures remain consistent interannually (Li et al., 2010). This, however, is not the case for salinity. Salinity shows small variations with changing seasons and substantial changes between yearly

averages (Li et al., 2010). Since stratification is controlled by salinity and temperature, the year-to-year variation in stratification in BB is therefore mainly correlated to yearly changes in salinity (Li et al., 2010) which correspond to yearly variations in precipitation and freshwater inputs (Shi and Wallace, 2018). Seasonal changes in stratification are more directly related to seasonal changes in water temperature which correspond to seasonal changes in air temperature. Seasonal stratification in the Basin occurs when temperatures at the surface start increasing around April. Stratification is then terminated during winter convection (i.e., from December to February) when surface water heat is lost to the air (Li and Harrison, 2008; Shan et al., 2011). These wintertime convection events homogenize the water column by combining the colder, fresher, and relatively oxygen-rich surface waters with bottom waters.

2.1.2 Seasonal Patterns of biogeochemical oceanographic conditions in BB

Oxygen concentrations on the surface of BB are mainly dictated by their exchange with the atmosphere. Since oxygen is more soluble in colder and saltier seawater, the highest concentrations of oxygen are observed in the last month/s of winter. After the occurrence of wintertime convection, oxygen concentrations in the water column are homogenized and subsurface oxygen concentrations increase (Shi and Wallace, 2018). Once the surface temperature increases during April and the spring bloom occurs, high export of phytoplankton-derived organic matter to the subsurface causes ammonium concentrations to increase due to the remineralization of organic nitrogen (Haas et al., 2021). This, in turn, causes a subsurface decline in oxygen concentrations because of respiration and nitrification. While the surface waters in the upper 20 to 30 m are connected to the outer harbour through the Narrows, during periods of strong stratification the bottom waters are essentially isolated from this surface circulation (Haas et al., 2022). Both the decline in oxygen and the isolation of the bottom layers allow for the development of hypoxic or even anoxic conditions in the bottom layer of the Basin (Platt and Conover, 1975; Hargrave et al., 1976; Punshon and Moore, 2004). During late summer, exports of organic matter decrease, and the rate of nitrification exceeds the rate of ammonium accumulation in the subsurface causing complete oxidation to nitrate (Haas et al. 2021). However, the timing and rate of nitrification are not consistent interannually due

to winter convection events on subsurface resident nitrifier concentrations. A strong dilution of these communities causes delays in nitrification on the scale of weeks to months regardless of the present concentrations of oxygen and ammonium (Haas et al. 2021).

2.2 Sources of observational data

The BBMP is a framework developed by the Bedford Institute of Oceanography (BIO) to acquire oceanographic data from the Basin (Therriault et al., 1998). Weekly measurements were collected using a Seabird SBE-25 CTD with an O_2 sensor at the BBMP station (44.689629°, -63.632756°) from 0 to ~70 m every 0.5 m (1999 - present). Moreover, water samples were collected at 4 discrete depths (1, 5, 10, and 60 m) using Niskin bottles to derive properties such as oxygen, chlorophyll, particulate organic carbon (POC), nitrate, salinity and more (1992 - 2022). Discrete water samples, however, were only available at 1, 5 and 10 m back in 1994, and both datasets have data gaps ranging from a week to a few months. Oxygen concentrations were derived from Niskin water samples by Winkler titration (2017 - present). Dissolved inorganic nitrogen (DIN) concentrations were measured using standard analytical methods for ammonium, nitrate, and nitrite. In this study, I will focus on temperature, salinity, oxygen, nitrate and ammonium.

2.3 Model Simulation

The model used is a multi-nested model simulation based on ROMS v.3.5 (Haidvogel et al., 2008). This physical model was modified from an earlier version of the physical model originally developed by Yi Sui in Jinyu Sheng's group (Sui 2023). The multi-nested model set-up is composed of 3 domains HRM1, HRM2 and HRM3 (Figure 2.1). Where HRM1 is the largest domain with the lowest resolution, and HRM3 is the smallest domain with the highest resolution. The HRM1 submodel has a resolution of ~885 m, and it uses open boundary conditions for ocean physical properties based on the global ocean reanalysis (GLORYS) and biogeochemical climatology from the Atlantic Canada Model (ACM; Rutherford et al., 2021; Laurent et al., 2021). For bathymetry, HRM1 uses the General Bathymetric Chart of the Oceans (GEBCO). The model results produced by HRM1 are used as open boundary conditions for HRM2, which

has a resolution of ~185 m and uses bathymetry from the Canadian hydrographic services for non-navigational purposes (NONNA). Submodel HRM3 is run similarly to HRM2 but using open boundary conditions based on the results produced by HRM2. Surface atmospheric forcing for all the submodels was obtained from the North American Regional Analysis (NARR). This type of communication between submodels is called one-way nesting and it only occurs in one direction (from a larger to a smaller domain). However, two-way nesting is also possible, where neighbouring submodels are sharing information from shared boundaries (in this case, the Narrows). In this thesis, I used the output from simulations of submodels HRM2 and HRM3 which were run from 2003 to 2023 by Arnaud Laurent. The one-way nesting HRM2 includes the Inner Scotian Shelf with 40 S-layers and 185 m horizontal resolution, this simulation will be referred to as HRM2. The two-way nesting HRM3 includes BB and the Narrows with 40 S-layers and a 61 m horizontal resolution. This simulation will be referred to as HRM23 because HRM2 and HRM3 were run together.

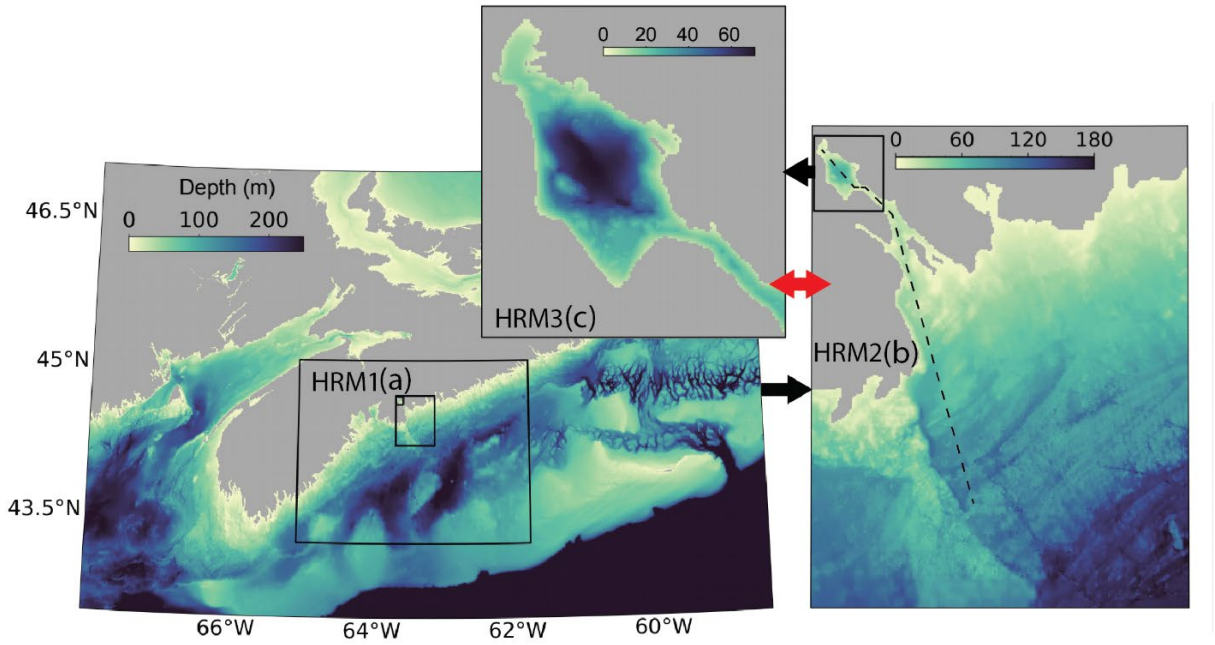

Figure 2.1. Multi-nested model set up for coastal waters around the HRM. Bathymetry map of the Scotian Shelf. The domains of **(a)** HRM1, **(b)** HRM2 and **(c)** HRM3 are delimitated by solid black lines. The domains and major bathymetry features of the Central Scotian Shelf (HRM1), the Inner Scotian Shelf (HRM2), and Bedford Basin and the Narrows (HRM3). The black arrows represent one-way nesting, and the red arrow represents two-way nesting. The dashed line represents the transect used in Figure 2.2.

Both simulations were analyzed and compared for intrusion events in the Basin. In addition, to imitate the data acquisition framework located at the BBMP station, the data used from the model simulations is the instantaneous daily model results. Moreover, the observations from the BBMP are only available every week on Wednesdays. Therefore, 2 datasets were created, daily model results, and weekly model results collected on Wednesdays. The former was used to characterize the intrusion events, and the latter was used to compare the model results with the observation from the BBMP station. The daily HRM2 model results were used to create 2 cross-sections of Halifax Harbour to highlight the model's ability to simulate these intrusion events (Figure 2.2).

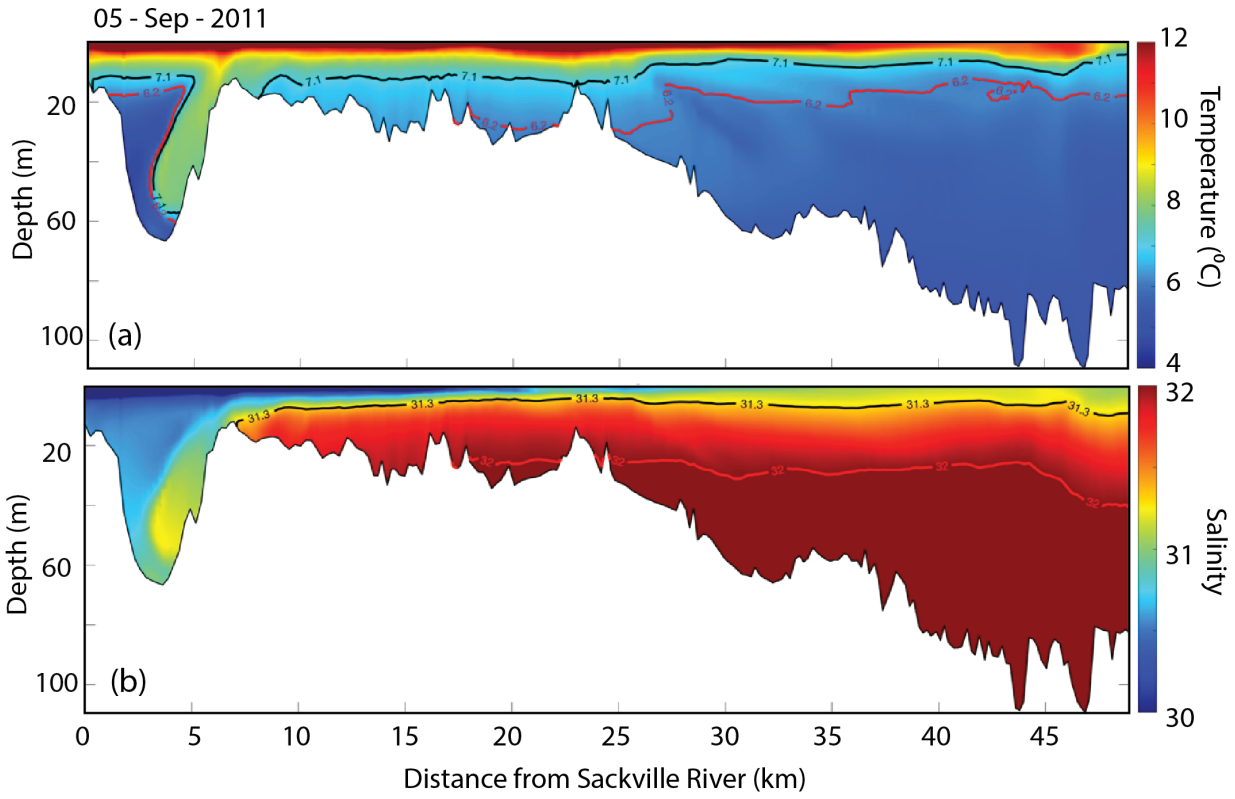

Figure 2.2. Cross-sections of **(a)** temperature and **(b)** salinity from the Halifax Harbour obtained from HRM2 on September 5, 2011. The transect line is shown in Figure 2.1.

2.4 Intrusion identification procedure

The visual identification of lateral intrusion events was carried out using measurements from CTD profiles and Niskin water samples. Since strong water intrusions have been observed at the bottom of the Basin, measurements below 60 m were used to calculate the depth average for each variable (except for the variables obtained from Niskin samples). Previous studies demonstrated that intrusion events cause a decrease in nitrate and an increase in temperature, salinity, density anomaly, and oxygen at the bottom of the Basin (e.g., Figure 2.3). These known effects were used to locate intrusion events in the BBMP dataset from 1999 to the present using time series and time-depth distributions of salinity (Figure 2.4). Moreover, time-depth distributions of salinity were used to study the effects of the intrusion events on the stratification of the water column and to separate intrusions from convection events. Winter convection events, like intrusion events, can cause sharp increases in oxygen and density at depth (Sui 2023). However, intrusion events are characterized by rapid increases in salinity while convection events are not. Making salinity the best variable for intrusion event identification at depth. However, an analysis performed on convection events in Appendix A shows that temperature and oxygen can be used to separate convection from intrusion events too.

For each intrusion event, the time between measurements (i.e., before and after intrusion) was recorded, and for each parameter, the change in magnitude per time step was calculated. It's important to mention that this method does not accurately quantify the immediate changes due to intrusion events since the time interval for the BBMP observations is 6 days. Most likely the temporal change in variables is due to a combination of different mechanisms, however, it is a good estimate for these changes using the observations available. This same procedure was performed on the HRM2 and HRM23 model simulations. However, these simulations do not possess estimates for the biological variables and therefore only temperature and salinity were used for identification. The information gathered from all the intrusions visually identified was used to characterize the frequency and effects of these events as observed at the BBMP station and to evaluate the performance of both model simulations at simulating intrusion events.

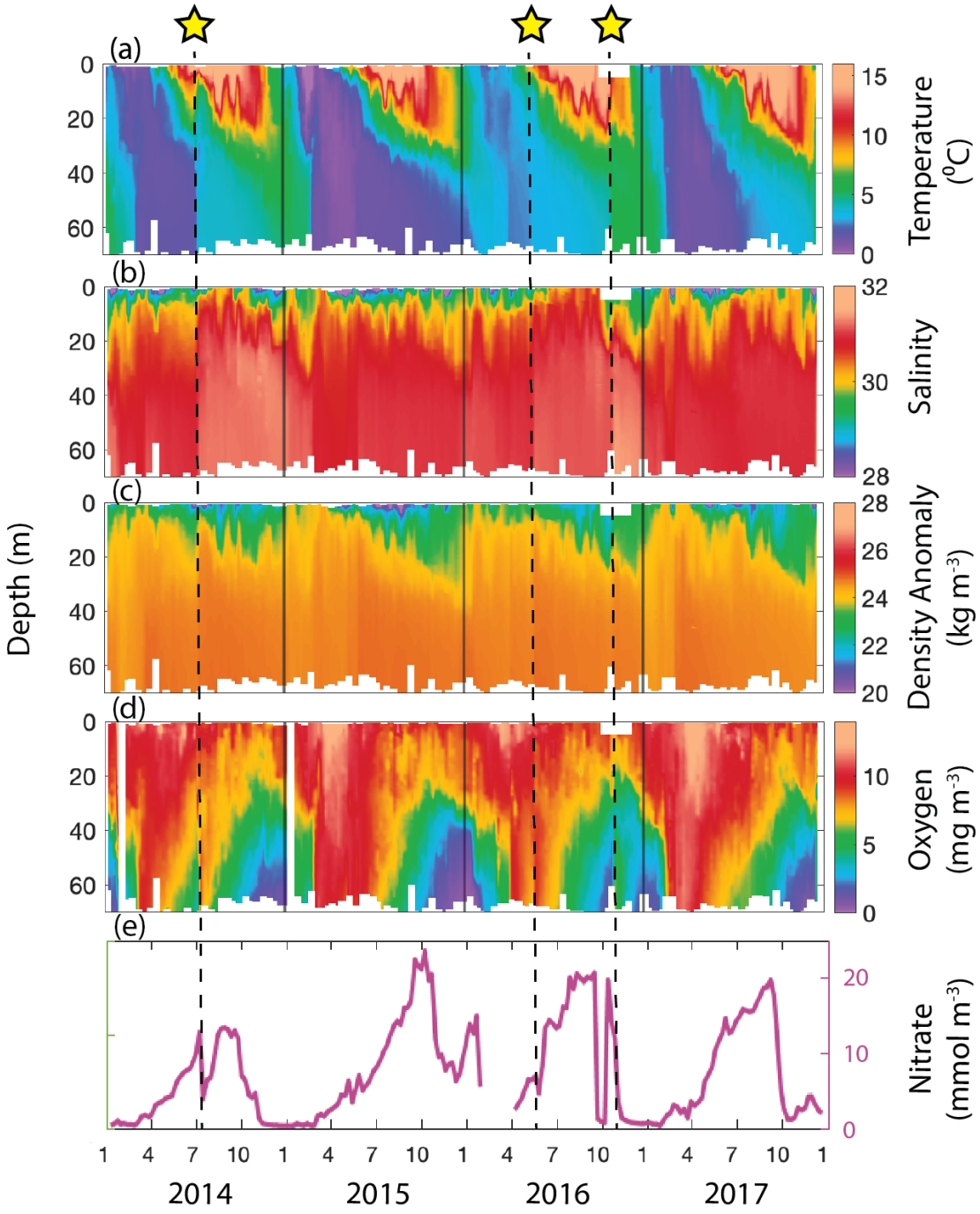

Figure 2.3. Time-depth distributions at the BBMP station for observed **(a)** temperature, **(b)** salinity, **(c)** density anomaly and **(d)** oxygen concentrations from January 2014 to December 2017. Time series average **(e)** nitrate concentrations below 60 m for the same period. The yellow stars mark the location of strong intrusion events.

2.5 Statistical methods for comparison

Comparison between model results and observations was carried out in 2 different ways. The average changes in temperature and salinity caused by intrusion events were calculated and compared between all the datasets. Moreover, the intrusion events identified in both the observations and the model results within 2 weeks of each other were identified. Since the measurements at the BBMP station are collected weekly, an intrusion identification at this station implies that there was an intrusion within the last week. On the other hand, on a daily data, we know that the intrusion events occurred within the last day. Therefore, the real separation between observed and simulated intrusions is 1 week. For instance, a simulated intrusion identified within 1 week ahead of the corresponding observed intrusion indicates that the maximum time difference between intrusions is 2 weeks due to the uncertain timing of the observed intrusion.

These events were used to calculate the model bias on the effects of strong intrusion events. This was performed to provide a more specific comparison between each event. The model biases were simply calculated as the difference between the effects simulated by the model and the effects measured at the BBMP.

2.6 Characterization of observed intrusions

One lateral intrusion event was identified on November 2, 2016 (Figure 2.5). This event represents an example of an intrusion event identification carried out on the BBMP dataset. In this example, the intrusion resulted in increases in temperature (~ 1.7 ºC), salinity (~ 0.32), and oxygen (~ 4.6 mg m-3), shown in Figure 2.5a. In addition, this event caused a sudden decrease in nitrate and ammonium (~ -6.7 mmol m-3 and ~ -8.3 mmol m-3, respectively), shown in Figure 2.5b. In terms of its effect on water stratification, this intrusion event was observed reaching from the bottom of the Basin up to ~10 m. Other intrusions with similar characteristics were identified from 2014 to 2020 and are highlighted in light pink in Figure 2.5. This identification was carried out for the entire BBMP dataset (see Appendix B). However,

the observations for 2020 contain gaps due to the COVID-19 pandemic and will be omitted for the rest of the thesis.

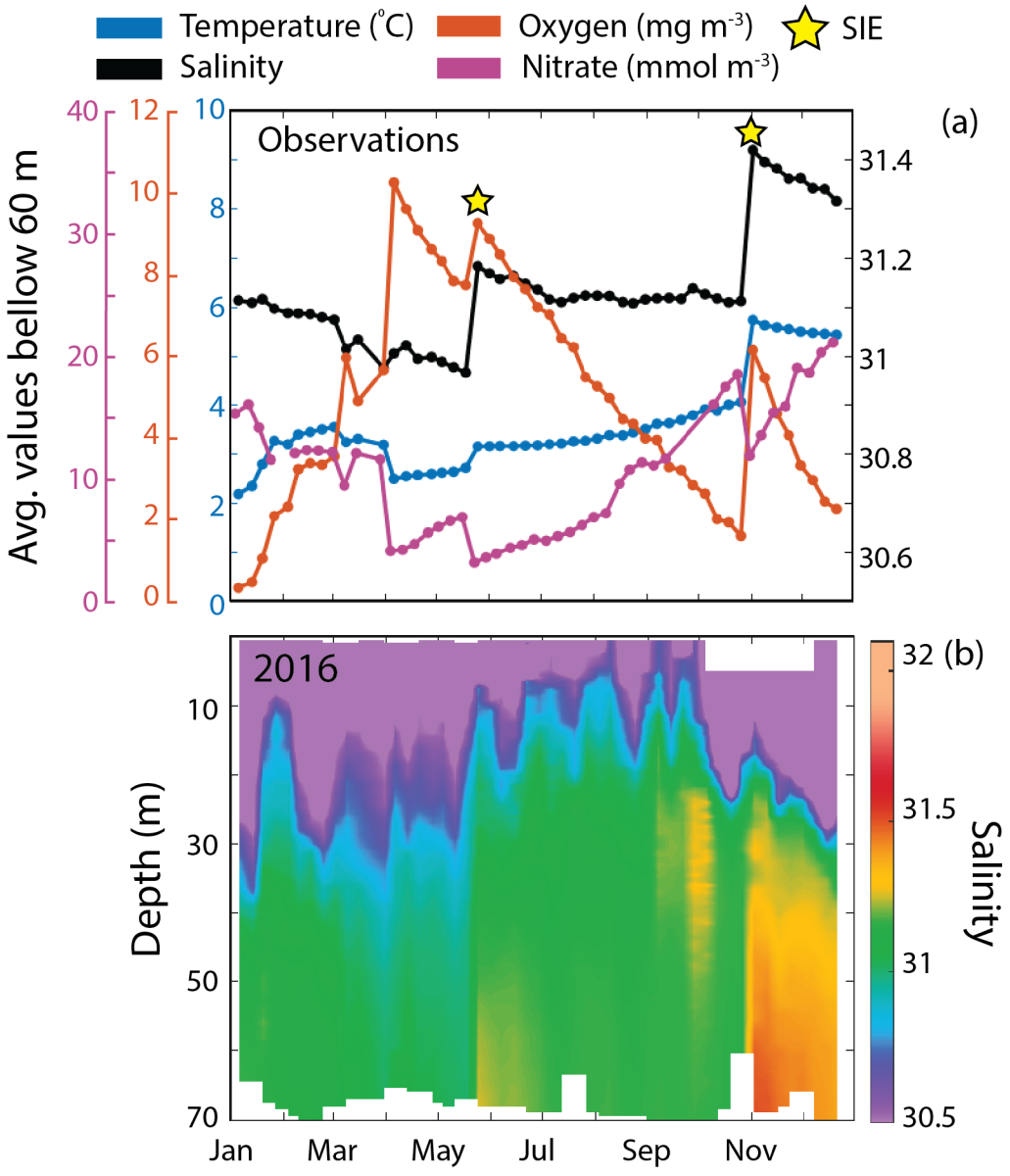

Figure 2.4. (a) Time series of average temperature (ºC), salinity, oxygen (mg m^{-3}), and nitrate(mg m^{-3}) below 60 m at the BBMP station**. (b)** Time-depth distribution of salinity. The yellow stars mark the intrusion event (SIE). These figures highlight the differences between convection (April) and intrusion events (May and November).

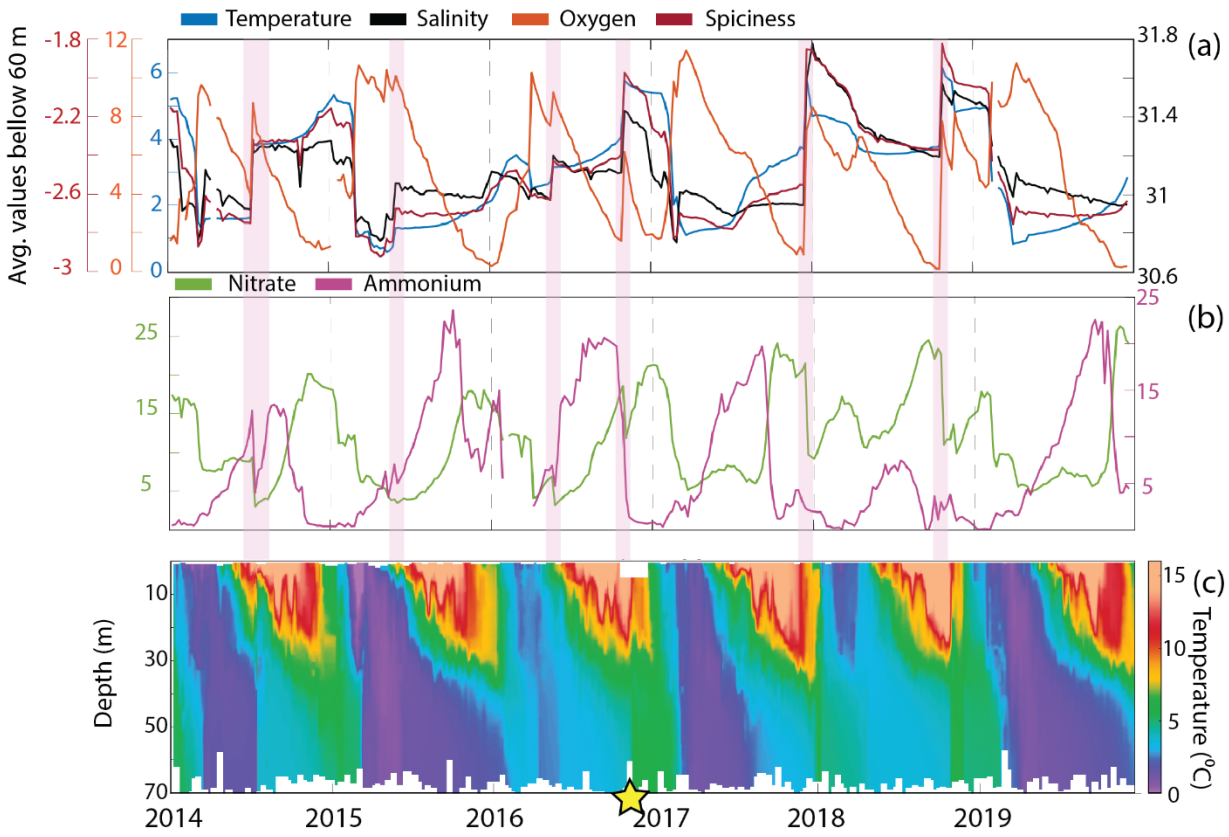

Figure 2.5. (a) Time series of average temperature (ºC), salinity, oxygen (mg m^{-3}) and spiciness below 60 m at the BBMP station from 2014 to 2020. **(b)** Time-series of nitrate (mmol m^{-3}) and ammonium (mmol m^{-3}) at 60 m. **(c)** Time-depth distribution of salinity. These figures were used to identify intrusion events (pink) in the BBMP data. The November 2, 2016, intrusion is marked with a yellow star.

A total of 29 intrusion events were identified in the BBMP dataset from 1999 to 2023. These intrusion events were separated into groups based on the time of the year they occurred, as shown in Figure 2.6a. In the observations two different groups of intrusions were identified, some occurring from April to July (i.e., spring/summer or SS intrusions) and some from September to December (i.e., fall intrusions). Strong intrusion events occurring from January to March (i.e., winter intrusions), if any, will be omitted in this study since their identification is more ambiguous than for the rest of the events. Moreover, these events were observed to occur most years (Figure 2.6b), and they are not restricted to one per year. Temperature increases due to intrusions reached an average of 1.24 ± 1.06 ºC/week, with SS intrusions affecting the temperature to a lesser extent (0.77 ± 0.57 ºC/week) than the fall intrusions (1.47 ± 1.18 ºC/week). A similar

trend was observed in salinity, with average increases of 0.32 ± 0.19/week for all the intrusions, 0.23 ± 0.15/week for the SS intrusions and 0.36 ± 0.20/week for the fall intrusions. Changes in oxygen concentrations averaged 3.48 ± 2.18 mg m^{-3}/week for all the intrusions, 1.56 ± 1.50 mg m^{-3}/week for the SS intrusions and 4.33 ± 1.88 mg m^{-3}/week for the fall intrusions.

Nutrient concentrations were also affected by the intrusion, causing decreases in nitrate of 6.08 ± 4.18 mmol m^{-3}/week for all the intrusions, 4.27 ± 3.95 mmol m^{-3}/week for the SS intrusions and 6.89 ± 4.13 mmol m^{-3}/week for the fall intrusions. In addition to changes in ammonium concentrations that varied from -2.97 ± 6.23 mmol m^{-3}/week for all the intrusions, -0.70 ± 4.72 mmol m^{-3}/week for the SS intrusions and -3.86 ± 6.63 mmol m^{-3}/week for the fall intrusions. Figures 2.6c and d are boxplots of the normalized changes in magnitude per week for temperature, salinity, nitrate, ammonium, and oxygen for intrusions occurring during spring/summer (SS) and fall, respectively. Each variable was normalized using 2 times the standard deviation of that variable below 60 m. These figures highlight the differences observed between SS and fall intrusion and it shows that fall intrusions tend to cause larger effects than SS intrusions. In other words, the fall intrusions cause larger increases in temperature, salinity, and oxygen, and larger decreases in nitrate and ammonium than SS intrusions. Moreover, using the intrusions observed at the BBMP station, the post-intrusion conditions were recorded and time-series of each variable were created to observe the changes in the disturbance caused by the intrusion event from 2000 – 2023 (see Appendix B).

Using plots of time-depth distribution of temperature, I was able to identify 3 different effects that intrusion events can have on the water column stratification at the BBMP station. Figures 2.7a, b and c are 3 time-depth distributions of temperature each representing different effects on the water column caused by intrusion events. Figure 2.7a represents an intrusion event that can be seen affecting the bottom of the Basin but does not homogenize the bottom layer (NH intrusions). In contrast, Figure 2.6b represents the intrusion events that cause complete homogenization of the bottom layer (H intrusions). Lastly, Figure 2.7c represents the intrusion events that not only homogenize the entire bottom layer but also homogenize the surface layer (F intrusions). This separation was no based on changes in temperature and salinity, but rather it was based

on the vertical extent of the intrusion events, and the conditions observed at depth after the event. Figure 2.7d is a stacked histogram of the number of intrusion events observed at the BBMP each month from 2003 – 2023 separated based on their effects on stratification. This figure shows that NH intrusion events occur early in spring (April and May), H intrusions can occur from April to October, and F intrusions occur in the last 2 months of the year. Overall, the BBMP dataset shows that the effect on the stratification of the water column caused by intrusion events increases from April to December. This could indicate that the velocity of the intrusion events increases from spring to winter, while also showing that the strong stratification present from spring to early fall limits the effects of the intrusion to the bottom layer.

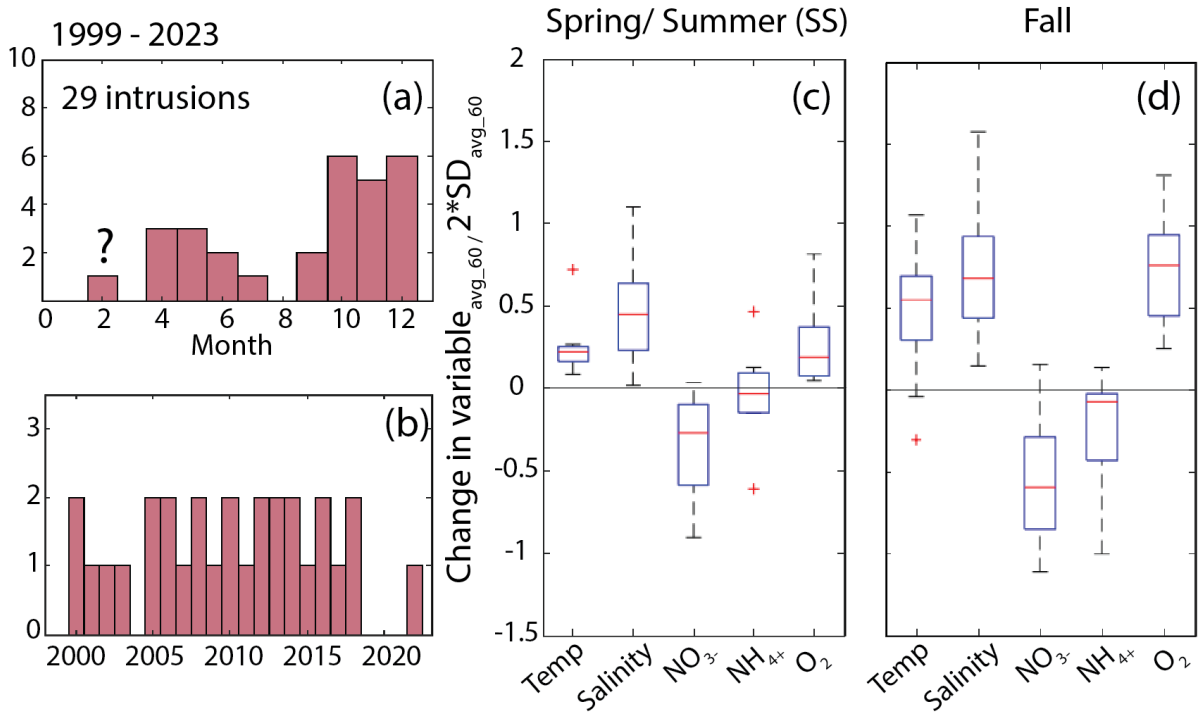

Figure 2.6. (a) Histogram of the total intrusion by month observed in the BBMP data. **(b)** Histogram of the number of intrusions by year from 1999 to 2023 (24 years). Boxplot of normalized changes in temperature (ºC), salinity, nitrate (mmol m^{-3}), ammonium (mmol m^{-3}), and oxygen (mg m^{-3}) for **(c)** SS intrusions and **(d)** fall intrusions. Values were normalized using two times their corresponding standard deviation (SD). The effects of intrusion events were normalized using 2 times the SD. The subscript 'avg_60' indicates that the values are depth averages below 60 m.

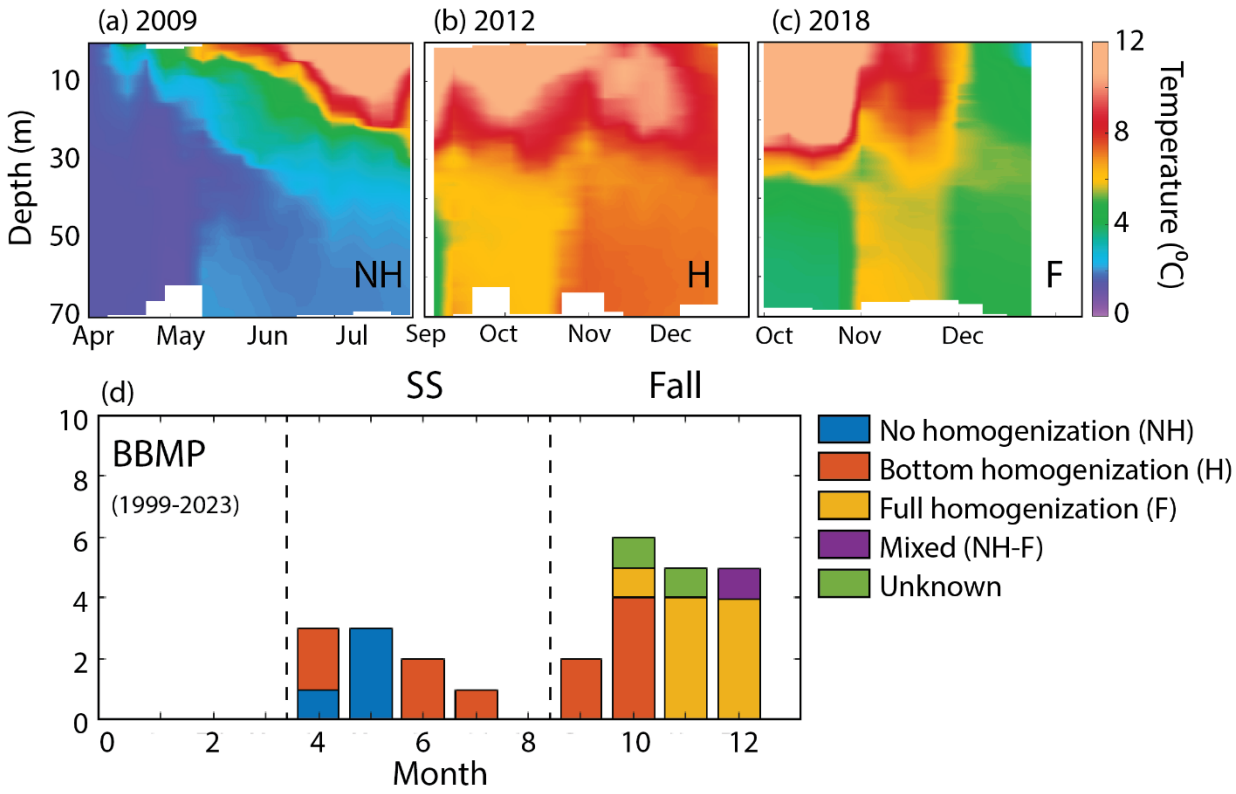

Figure 2.7. Time-depth distributions of temperature in **(a)** 2009 representing NH intrusions, **(b)** 2012 representing H intrusions, and **(c)** 2018 representing F intrusions. **(d)** Histogram of intrusion events in the BBMP from separated based on the effects on water column stratification. NH-F is a combination of NH and F, and O indicates the unresolved effects.

2.7 Comparison between intrusion events present in HRM2, HRM23, and the BBMP datasets

The same procedure for intrusion identification explained in the previous section was performed on both HRM2 and HRM23. However, these simulations do not have estimates for oxygen, ammonium and nitrate and therefore only temperature and salinity were used for identification and comparison. Figure 2.8 is composed of 3 histograms of the number of intrusion events per month from 2003 – 2023 for all the datasets. The number of intrusion events observed in HRM2 and HRM23 are 52 and 28, respectively. Since only 25 events were observed in the BBMP dataset, this indicates that both simulations overestimated the number of intrusion events, especially HRM2 with more than double the observed number of events. Moreover, this figure shows that the separation between SS and fall intrusion observed in the BBMP dataset

is still present in HRM2 and HRM23. However, in HRM2 there are at least 3 times the actual number of intrusions observed from April to July. Overall, HRM2 overestimates the number of intrusion events perhaps highlighting issues related to the density conditions of both the pre-existing and the intruded water. In the HRM23 model simulation, the separation between the SS and fall intrusions is not as clear as in HRM2 and BBMP. In HRM23 intrusion events occur almost every month of the year and the large number of intrusions in October and November present in the BBMP dataset are underestimated. The average effect of the intrusion events at the BBMP station was compared to those observed in the model simulations. Figure 2.9 shows 2 boxplots comparing the effects on temperature and salinity observed in HRM2, HRM23, and BBMP. Overall, the only clear difference between HRM2 and HRM23 is the stronger differences between fall and SS intrusion observed in HRM23. Which is more concordant with what is present in the BBMP dataset. However, both model simulations overestimate the effects of intrusion events occurring throughout the year.

The intrusions simulated in both HRM2 and HRM23 were characterized using the same categories mentioned in section 2.6 for effects on stratification. The results are shown in Figure 2.8 where I compare the results of this characterization between model simulations and BBMP observations. This figure highlights the underestimation of bottom water homogenization caused by intrusion events in both models. Only 12% of the intrusion events in the BBMP were categorized as NH, while this number increased to 65% - 75% in the model simulations. In the BBMP dataset, this category of intrusions was only observed during spring and summer. However, in the simulations these occur throughout the year, especially in HRM23. Perhaps indicating an overestimation of the density stability of the bottom water of BB which would cause an underestimation of the enhanced mixing initiated by intrusion events.

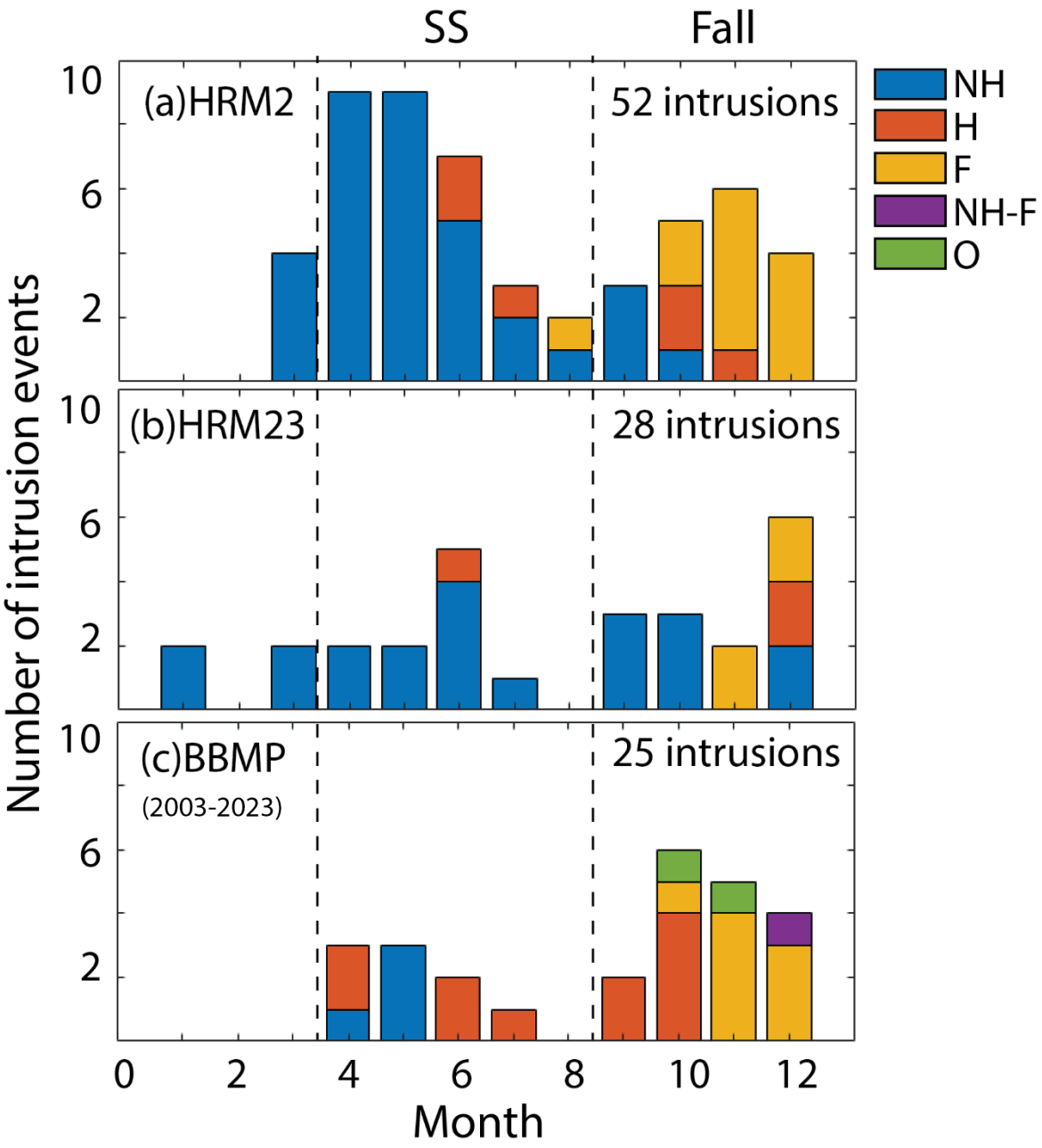

Figure 2.8. Histogram of the total intrusion by month observed in the **(a)** HRM2, **(b)** HRM23 and **(c)** BBMP data from 2003 – 2023 (20 years). Intrusion events were separated based on the effect on water column stratification. Based on the categories in Figure 2.7.

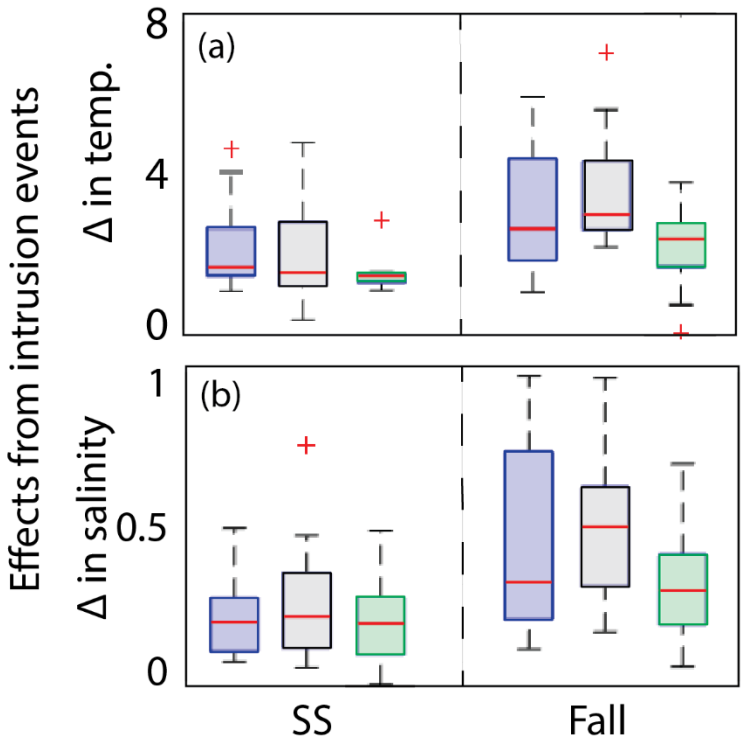

Figure 2.9. Boxplots of the effects on **(a)** temperature and **(b)** salinity caused by intrusion events separated by spring/summer and fall for HRM2 (blue), HRM23 (black), and BBMP (green).

Further comparison between model results and observations was carried out by identifying intrusion events in both datasets that occurred within 2 weeks of each other. These pairs of intrusion events were compared by subtracting the changes in temperature and salinity measured in the simulation and those measured in the observations. In other words, the model bias was calculated for both HRM2 and HRM23 in terms of the effects caused by intrusion events. Figure 2.10 is composed of 2 scatter plots where the x-axis represents the temperature bias, and the y-axis represents the salinity bias in the simulations. The intrusion events in these plots were separated into SS (blue) and fall (red) intrusions. These plots allowed me to separate the intrusion events into quadrants and further characterize the performance of the simulations. The results indicate that overall, both simulations are performing similarly in terms of the effects caused by intrusion events. Both simulations show the overestimation of both temperature and salinity for fall intrusion events. The HRM2 simulation tends to overestimate the temperature and salinity

conditions of SS intrusions, while the HRM23 tends to underestimate them. Figure 2.11 is composed of 2 pie charts that represent the intrusion events that were simulated within 2 weeks from the real intrusions in the BBMP dataset for both HRM2 and HRM23. The pie charts are separated into categories, correctly identified (dark blue), erroneously simulated as mid-depth intrusions (light blue), intrusion events with negative change in temperature, salinity or both (green), and the events missed (yellow). This figure shows that HRM23 performs better than HRM2, since HRM23 only missed 12% of the intrusions, whereas HRM2 missed 32%.

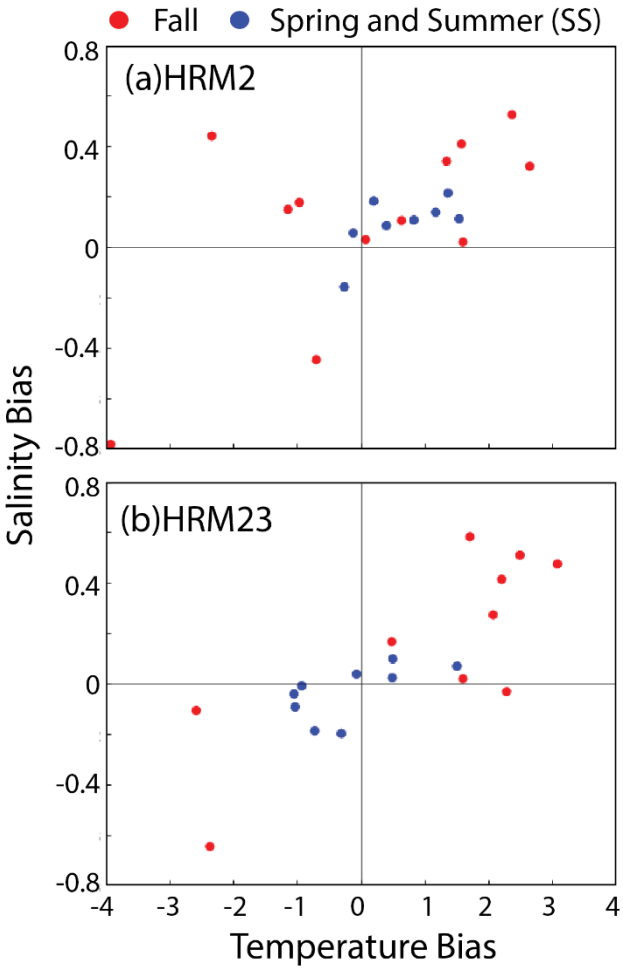

Figure 2.10. Scatter plot of the bias in changes in temperature and salinity observed in **(a)** HRM2 and **(b)** HRM23. Where the red dots represent fall intrusions and the blue dots represent spring/summer intrusions.

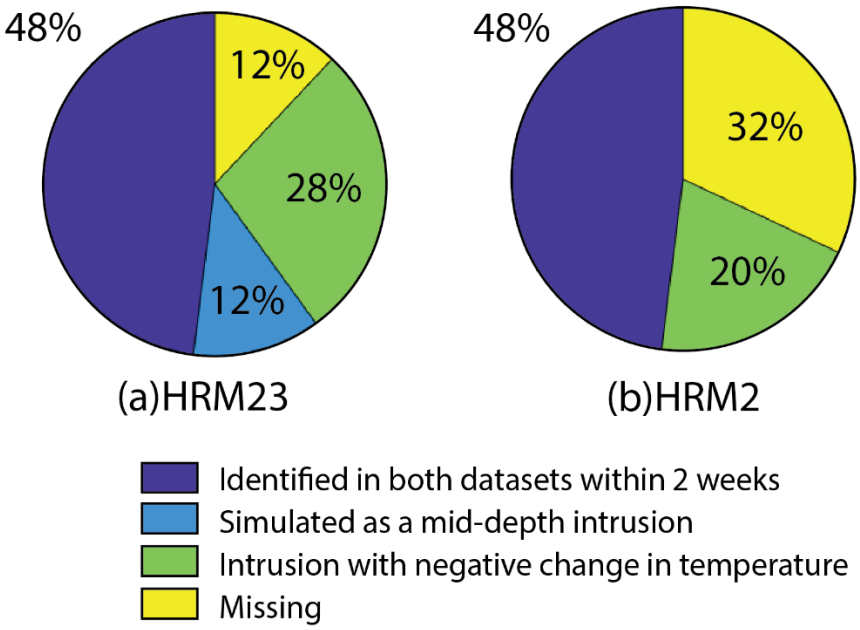

Figure 2.11. Pie charts representing the comparison between the identification of intrusions in the BBMP and each of the model simulations, **(a)** HRM23 and **(b)** HRM2. Where dark blue, light blue and green represent intrusion events identified within 2 weeks from each correctly, erroneously simulated as mid-depth intrusion events, and erroneously simulated with negative effects in temperature, respectively.

2.8 Summary and Discussion

Strong lateral intrusion events are dense water masses that cause rapid changes in the oceanographic properties of the surrounding bottom water in BB. From 1999 there is a record of 29 possible intrusion events in the BBMP dataset (not accounting for 2020 due to lack of enough data). These events cause increases in temperature (1.24 ± 1.06 ºC/week), salinity (0.32 ± 0.19/week), and oxygen (3.48 ± 2.18 mg m^{-3}/week) and decreases in nitrate (-6.08 ± 4.18 mmol m^{-3}/week) and mostly decreases in ammonium (-2.97 ± 6.23 mmol m^{-3}/week). The majority of intrusion events occurred during fall, but some events were also observed during spring and summer. Intrusions occurring in the fall caused larger disturbances than intrusions occurring earlier in the year for all variables, but most importantly oxygen. This is likely due to the seasonal depletion of oxygen at depth from water column respiration. In other words, earlier during the year the oxygen concentrations at depth are higher than during October since more water column respiration

has occurred. Therefore, intrusion events occurring later in the year would cause larger increases in oxygen than during spring. Moreover, fall intrusions were shown to have larger effects on the stratification of the water column. As the year progresses, the intrusions start by only partially affecting the bottom later. Halfway through the year, the events start affecting the entire bottom layer and by the end of the year, these events are affecting both bottom and surface layers. This could be caused by an interaction of mechanisms such as the weakening of the stratification late in the year and the possible increase in the velocity of the intrusions from September to December. All these factors indicate that the intrusions interacting with the BB during the fall play a larger role in deep water renewal than spring/summer intrusions. These findings are concordant with previous findings by Sui (2023), where he was able to show that natural variability in wind velocities in the area can cause SS intrusions to have a lesser impact than fall intrusions in BB. Notice that the prevailing winds during fall are northwesterly and these do not flow parallel to the coastline. This implies that upwelling is likely not the only mechanism for intrusion events into BB. The wind direction plays a role in defining the strength of the estuarine circulation of the Halifax Harbour (HH) and, in Sui (2023), it was shown that northwesterly winds enhance this circulation, while southwesterly do the opposite (characteristic for summer/spring). Therefore, the circulation of the HH plays an important role.

Intrusion identification was also carried out in the HRM2 and HRM23 model simulations. Both simulations were able to represent the trend in number of intrusion events per month observed in the BBMP dataset, but the total number of intrusions was overestimated, especially SS intrusions in HRM2. The higher resolution HRM23 model simulation showed more similarities with the BBMP dataset, including the differences between fall and SS intrusion events. In terms of the effects on water column stratification, the HRM2 outperforms the HRM23 showing similar patterns during fall as observed in the BBMP. However, overall, both simulations have model deficiencies in underestimating the vertical mixing at depth caused by the intrusion events. The HRM23 simulation missed 12% of the intrusions present in the BBMP, while 32% were missed in the HRM2. Moreover, HRM23 tends to erroneously simulate mid-depth intrusion

events where there should be deep intrusion events during fall. Overall, HRM23 performs better than HRM2, and therefore HRM23 was used for the model experiments performed in Chapter 3.

CHAPTER 3

EXPERIMENTS WITH MODEL SIMULATION

This chapter describes the intrusion identification method used on the HRM23 model simulation and the observational data from BBMP. This includes a description of the intrusion identification algorithm, and the optimization method used to estimate the site-specific changes in temperature and salinity characteristic of intrusion events at the BBMP station. Moreover, 2 experiments using HRM23 were carried out. The first experiment evaluates the reliability of weekly observations at identifying intrusion events by comparing the effects caused by these events from both daily and weekly model results. The second experiment analyzes the intrusion events as they advance landward using a longitudinal cross-section of the Basin. The objective of the second experiment is to evaluate whether all the intrusion events affecting the Basin are recorded at the BBMP station. Lastly, in this chapter, the intrusions simulated and the intrusion observed in the BBMP dataset are further compared.

3.1 Algorithm description

To characterize and identify intrusion events in a time series of water column profiles, a methodology was developed using MATLAB R2023a. This algorithm was designed to analyze changes in both salinity and temperature at specific depths after 1 timestep (in this case, weekly or daily). The depth chosen for identification depends on the maximum depth of the profiles in question, which will change as the location of the profile changes. The algorithm was designed to handle data of any time resolution, and therefore the units of time will depend on the data. It operates by iterating through the time series. For each timestep, the algorithm analyzes the observed changes in salinity and temperature. When the algorithm detects changes that exceed predefined thresholds for both salinity and temperature, it flags the corresponding time point as a potential intrusion event.

In addition to the thresholds for temperature and salinity, the algorithm requires 2 parameters that help handle high-resolution data (e.g., daily data). The first parameter *ddays* is used to account for intrusions that are separated by one or two days. This prevents the script from separating one intrusion event into what appears as 2 events. The second parameter, *tale*, is related to identifying when the effects of the intrusion events start and end. This algorithm works by identifying changes in a variable that exceed a certain threshold, however, these effects do not always represent the total change in temperature and salinity caused by an intrusion event. These may only represent the fastest change in variables observed in the intrusion. For this reason, to estimate the total change in variables it is necessary to identify the 'tails' of the intrusion event (i.e., the observed effect before and after the fastest rate of change per intrusion). However, the extent of the 'tails' is normally obscured and combined with other background mechanisms which makes it difficult for the algorithm to bypass. Therefore, the second parameter is represented through the following equation:

$$tale = \Delta v_{day} / min\Delta v_{day} \quad (1)$$

Where Δv_{day} represents the change in variable per day flagged by the algorithm, and $min\Delta v_{day}$ represents the minimum change in variable per day allowed to be part of the flagged event's 'tails'. The parameter *tale* defines the minimum ratio of the fastest rate of change within the intrusion in question that can be identified as part of its 'tail'. While this parameter does not ensure that the total change is recorded, it allows it to maximize the ratio that it does record. The values used in this thesis for *ddays* and *tale* were chosen based on the performance of the identification algorithm, and the final values are 1 day and 0.3, respectively. In other words, single intrusion events are allowed to be discontinuous by 1 day and the timesteps that correspond to the 'tails' are allowed to have changes in variables larger than $0.3\Delta v_{day}$. Notice that this will only apply to the daily data.

3.2 Optimization of salinity and temperature thresholds

This intrusion identification algorithm allows for the systematic and consistent identification of intrusion events, reducing potential observer bias and facilitating a comprehensive analysis of the frequency and characteristics of these events. However, since the script relies on inputs for the salinity and temperature thresholds, these values need to be estimated before a reliable identification can be performed. This is where the visual identification of intrusion events in the observation and the simulations becomes relevant since we can use this information to determine the best threshold values for each dataset. These values can be estimated by using an optimization function that uses performance parameters to identify the best threshold values based on the visual identification of intrusion in the dataset. The performance parameters chosen for the optimization function were *error* and *extra*. Both parameters were combined into a single parameter named '*Total error'*.

$$error = OI_{missed}/OI_{all} \quad (2) \qquad extra = AI_{only}/AI_{all} \quad (3)$$

$$Total\ error = error + 0.5extra \quad (4)$$

Where OI_{missed} is the number of manually identified intrusions that were missed by the algorithm, OI_{all} is the total number of manually identified intrusions, AI_{only} is the number of intrusions only identified by the algorithm, and AI_{all} is the total number of intrusions identified by the algorithm. In equation 4, *extra* is multiplied by 0.5 as a weighting factor to prioritize the identification of as many visually identified intrusions as possible. By minimizing *total error*, the best salinity and temperature thresholds for identifying intrusion events can be estimated. For the optimization, the intrusion identification algorithm was automatically tested using different variations of the salinity and temperature thresholds from 0 to 1 unit with intervals of 0.01 units for each variable. In other words, every 100 iterations the salinity threshold increases by 0.01 PSU, and in every iteration, the temperature threshold increases by 0.01 ºC for every 100 iterations. The combination of thresholds that results in the lowest value for *total error* are selected as the optimized thresholds for the dataset in question (Figure 3.1).

3.2.1 Results

The optimized salinity and temperature thresholds to identify intrusion events in the HRM23, and in the BBMP datasets were estimated. The resulting optimized thresholds for the BBMP and the HRM23 were 0.07 /week for salinity and 0.26 ºC /week for temperature. Using these numbers, I was able to identify 80% of the intrusions in the BBMP. The other 20% were "intrusion events" occurring in winter, or unique events where the temperature decreased after the intrusion occurred. These numbers also resulted in 4 extra intrusions identified in the BBMP dataset, all of which were "winter intrusions". This same pattern was also observed in the HRM23 simulation. This was corroborated by identifying the optimization thresholds for the weekly and daily resolved data from HRM23. This resulted in the same thresholds and the same 20% of intrusions missed, but the daily data contained 12 more extra intrusion events than the weekly data.

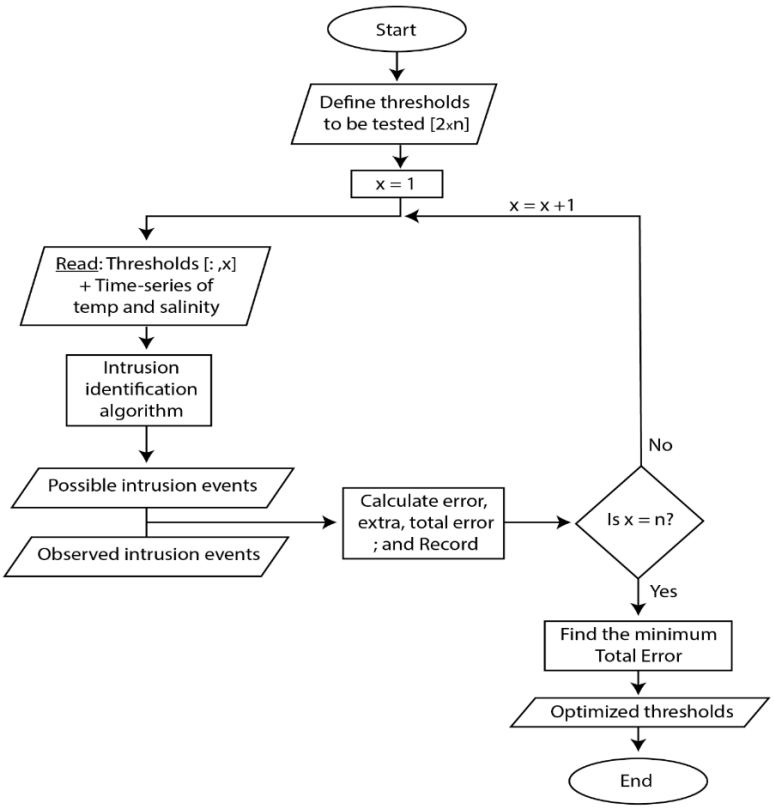

Figure 3.1. Flow chart showing the steps taken to obtain the salinity and temperature thresholds characteristic of intrusion events in BB. Where 'n' is the number of pairs of thresholds to be tested, and 'x' acts as an iteration variable that specifies the algorithm to move on to the next pair of thresholds or to stop and identify the best thresholds from the ones already tested.

3.3 Algorithm performance comparison between datasets of different resolution

Intrusion identification was carried out in the daily and weekly model results from HRM23. The weekly data analysis involved the identification of intrusion events in 7 different datasets. Each data set contains weekly data collected on different days of the week. So far, I have been using the weekly dataset collected on Wednesdays. The analysis was done to compare the number and the effects of intrusion events in the daily and weekly model results. In all the weekly datasets, the same number of intrusion events were recorded as in the daily model results. These findings indicate that most of the intrusion events in BB can be identified using a weekly data acquisition scheme at the BBMP station.

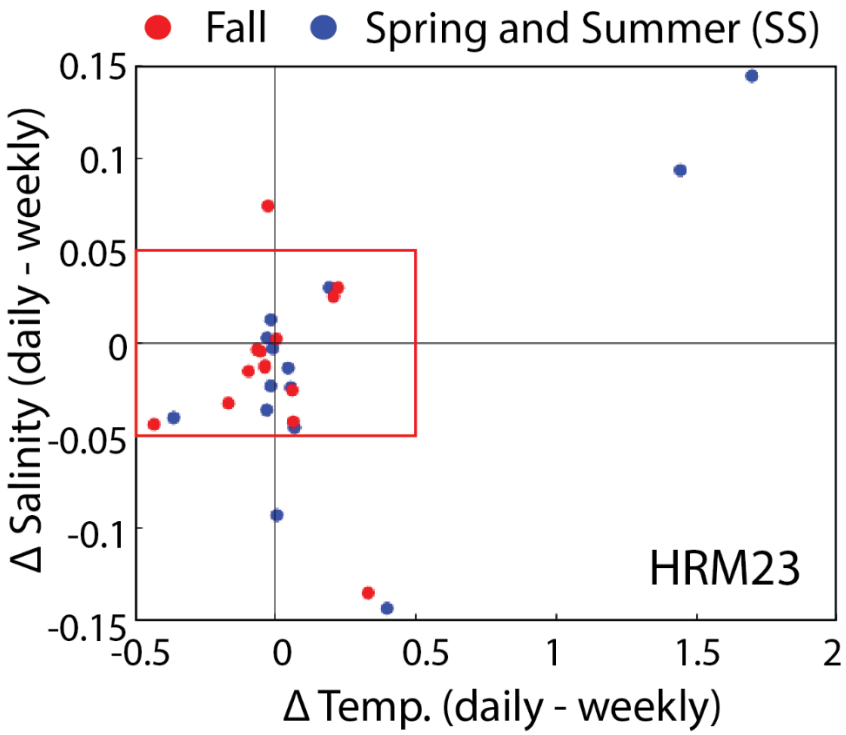

Figure 3.2. Scatter plot of the differences in changes in temperature and salinity observed in daily and weekly resolved data from HRM23. Where the red dots represent fall intrusions and the blue dots represent spring/summer intrusions. The red box highlights the majority of the datapoints.

The differences in the effects observed in the daily and weekly model results were calculated and compared. Figure 3.2 is a scatter plot where the x-axis represents the differences in the effects on temperature, and the y-axis represents the differences in the effects on salinity between daily and weekly model results from the HRM23. In addition, the intrusions have been separated into SS (blue) and fall (red) using colours. The intrusions in HRM23 have an average effect in temperature and salinity of 1.8 ºC and 0.4, respectively. In this figure, there is a red rectangle that surrounds the majority of the intrusion events present in HRM23. This rectangle highlights that the majority of the intrusions observed in the weekly data are being overestimated or underestimated in comparison to the effects observed in the daily data. Where the intrusions in the weekly data can differ in temperature and salinity by 27% and 13%, respectively. Moreover, the intrusion events surrounded by the red box represent 80% of the events. The other 20%, mainly composed of SS intrusions, resulted in larger differences for temperature and salinity of up to 65% and 38%, respectively. These results indicate that while all the intrusion events can be identified using weekly data, the effects of these events tend to be overestimated in comparison to daily data.

3.4 Intrusion continuity analysis

One of the limitations of the observational data is that it is restricted to a single location. Since the model simulation covers the entire Basin, 4 locations were selected for intrusion identification (Figure 3.3). These stations are arranged in a line. Station 1 (ST1) is the station closest to the Narrows, with a distance of ~1.35 km from the MacKay Bridge. This station is located at (44.684871°, -63.625995°) with a maximum depth of 45 m. Station 2 (ST2) is the second station of the transect moving landwards. This station is located at (44.676562°, -63.607468°) with a maximum depth of 59 m. Station 3 (ST3) is the BBMP station with a maximum depth of 70 m, and station 4 (ST4) is the station closest to the Sackville River, located ~3.55 km from the MacKay Bridge (44.699151°, -63.646002°) with a maximum depth of 61 m. Between ST1 and ST4 the distance between the stations is constant (~ 750 m). The identification algorithm was used on all the new stations. The intrusion events observed at each station were connected to intrusions observed at other stations using the date at which they were observed. This resulted in intrusions that can be tracked

along the transect. With this information, I was able to categorize the intrusion events in BB based on their extent along the Basin. The different categories are low (events only reaching ST1), moderate (ST2), high (ST3), and full (ST4) reach intrusion events.

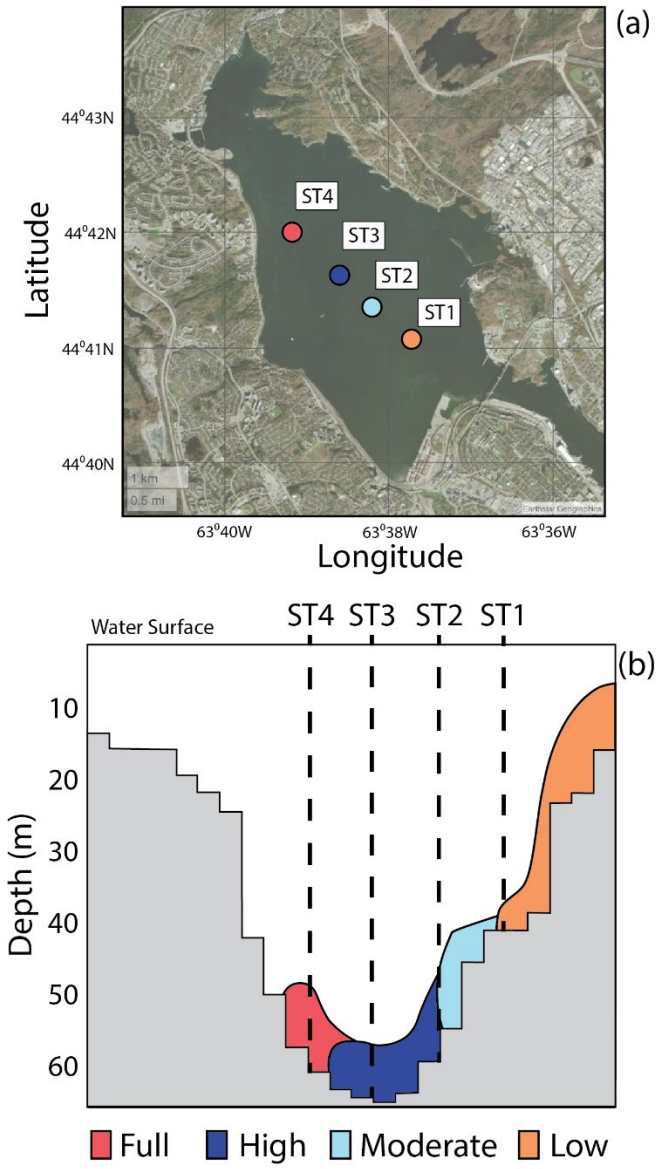

Figure 3.3. a) Satellite map of the Bedford Basin and the surrounding area. Circles represent the added stations. **b)** Cross-section of the Bedford Basin where the location of the stations is marked with dashed lines and the different categories (i.e., full, high, moderate, low). This diagram is a schematic visually based on model results.

The analysis resulted in the identification of 19 full, 2 high, 1 moderate, and 12 low reach intrusion events. These results indicate that intrusion events that make it to the Basin are either trapped at ST1 (35% of the intrusions) or reach up to ST4 (56% of the intrusions). This implies that not all the intrusion events affecting the Basin reach the BBMP station. Only the events that make it to the bottom of the Basin are recorded in the BBMP. Moreover, these intrusion events can be further categorized based on their approaching speed. Based on the intrusions identified in this section, 3 different groups of events were identified based on their approaches to the Basin. Figure 3.4 shows 4 temperature and salinity time series at four stations in BB, each marked with the corresponding station from where the data was obtained. In this figure, an example of a slow-approaching intrusion event is shown. This characterization is based on the time it took for the effects of the intrusions to be fully present in ST1. Notice that in this case, this took longer than half a month. An example of a fast-approaching event is shown in Figure 3.5. In contrast to the slow-approaching events, these take less than a few days to fully affect ST1. And lastly, the approach of multi-step intrusion events (Figure 3.6) can be characterized as fast, however, it also shows that the intrusion event got stuck in ST1 for almost 2 weeks before continuing to ST4. These categories were used to categorize the intrusion events and observe how these are temporally distributed thorough the year (Figure 3.7). The results indicate that the speed at which the intrusion events approach the Basin increases from February to December. The shift from slow to fast-approaching intrusions appears to start during July. However, if we take a look at the histogram for HRM23 in Figure 2.8, we can see that a lot of the intrusions from July to October in Figure 3.7 do not make it to the BBMP. What this implies is that at the beginning of the year, the intrusions approach slowly to the Basin. During July these intrusions start becoming faster but do not make it to the bottom of the Basin. During October the events start becoming fast enough to bypass ST1 and rapidly make it to ST4. Finally, at the end of the year, the intrusions start to slow down again and these become multi-step intrusion events. Overall, this indicates that the velocity of the approach of an intrusion event increases from February to December and then they slow down from December to February. Take into consideration that just because the approach of the events is slow does not mean that

the intrusion won't make it to ST4. Slow-approaching events can affect ST4 by building up intruded water at ST1 and eventually overflowing towards ST4.

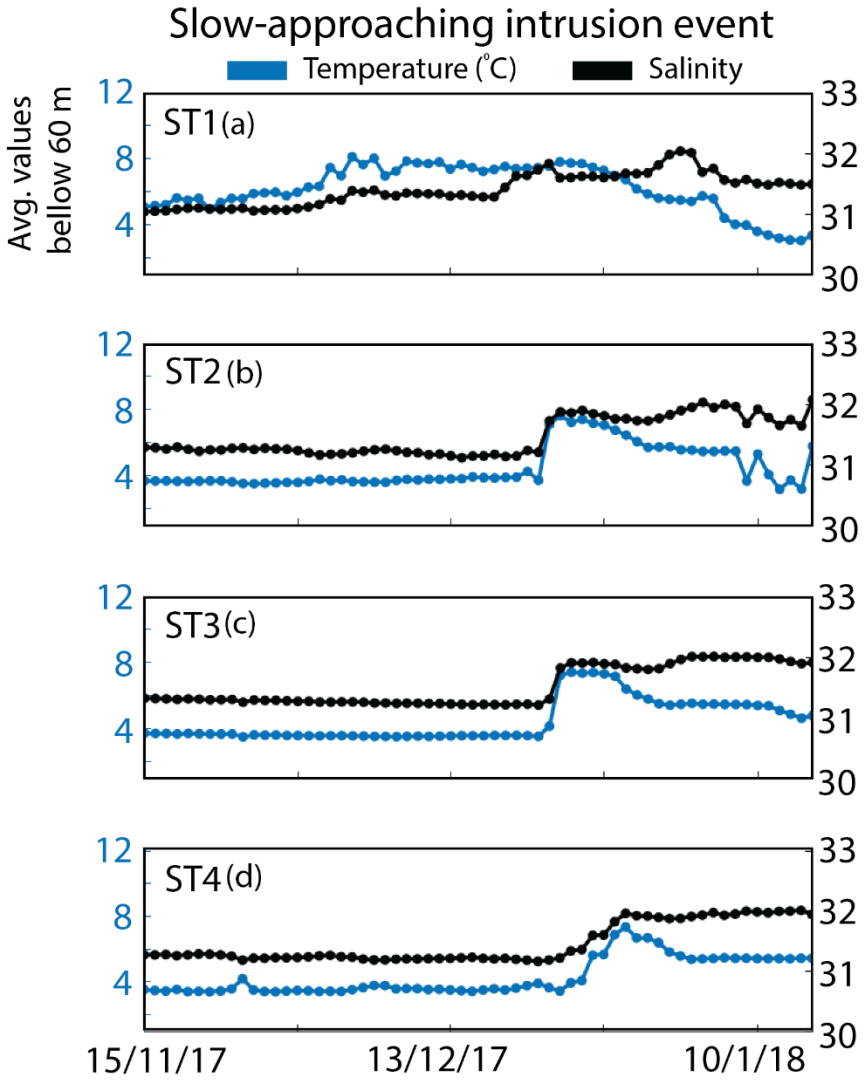

Figure 3.4. Time series of average temperature (ºC) and salinity below 60 m at four stations in BB; **(a)** ST1, **(b)** ST2, **(c)** ST3, and **(d)** ST4. This figure shows an example of slow-approaching intrusion events.

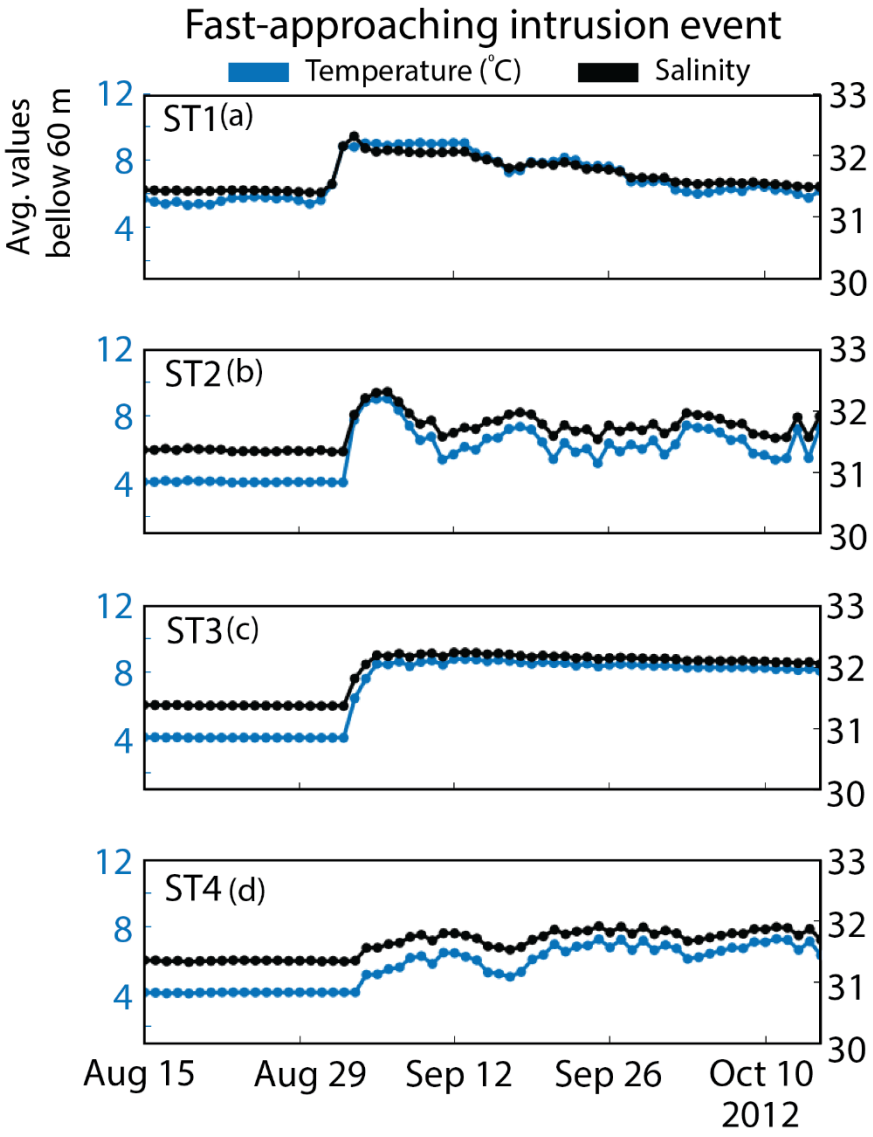

Figure 3.5. Time series of average temperature (ºC) and salinity below 60 m at four stations in BB; **(a)** ST1, **(b)** ST2, **(c)** ST3, and **(d)** ST4. This figure shows an example of fast-approaching intrusion events.

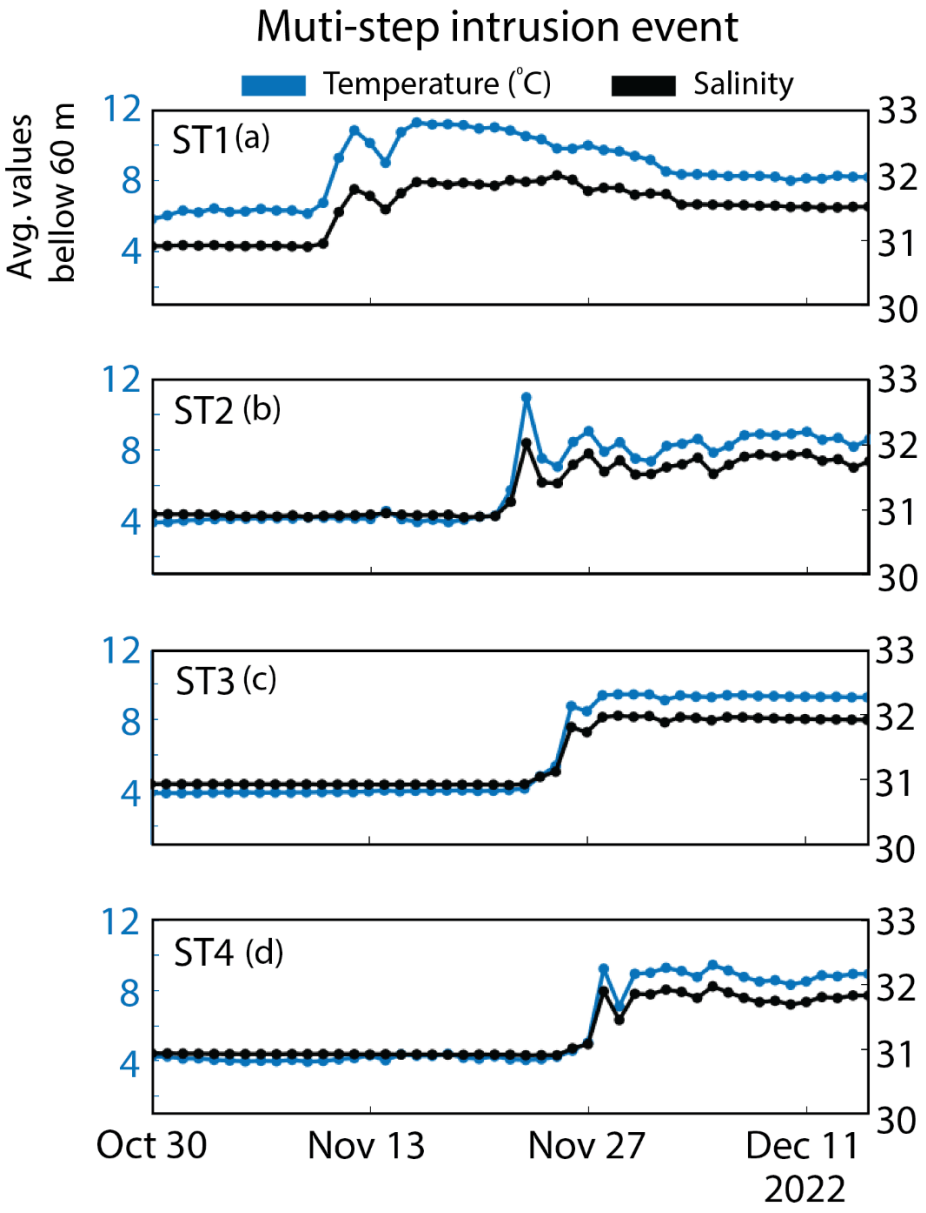

Figure 3.6. Time series of average temperature (ºC) and salinity below 60 m at four stations in BB; **(a)** ST1, **(b)** ST2, **(c)** ST3, and **(d)** ST4. This figure shows an example of multi-step intrusion events.

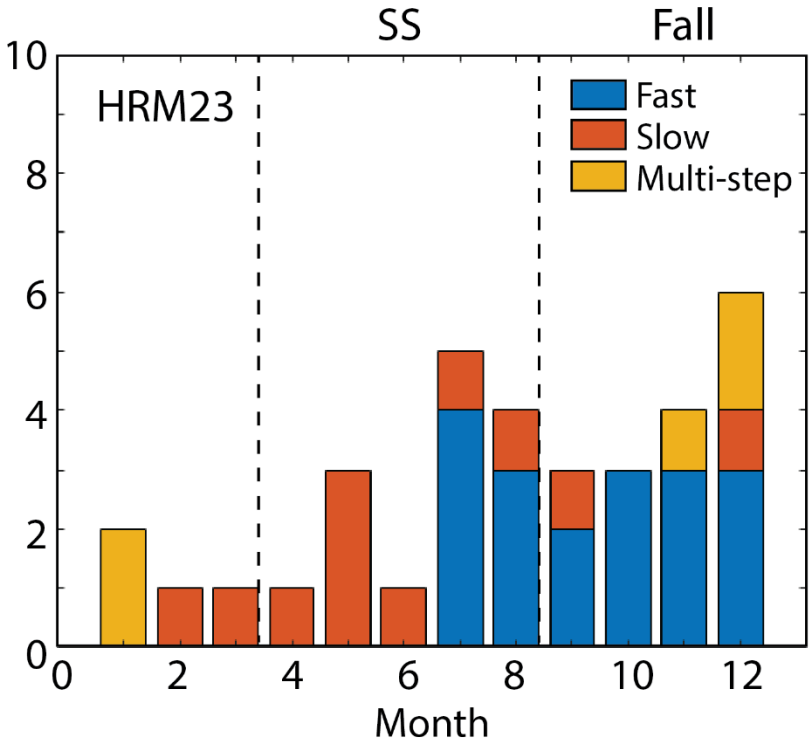

Figure 3.7. Histogram of the intrusions identified in the continuity analysis from HRM23. These intrusions were separated based on the speed of their approach to the Basin. This includes intrusions that did not make it to ST3/the BBMP station.

3.5 Summary and Discussion

A methodology was developed in MATLAB R2023a to systematically detect rates of change that exceed predefined thresholds for both salinity and temperature characteristics of strong intrusion events in a dataset. These thresholds were estimated for both the BBMP dataset and HRM23. The resulting thresholds for both datasets were the same (0.07 /week and 0.36^{o}C /week). The methodology, in combination with the thresholds calculated, was able to identify the majority of the intrusions visually identified in Chapter 2 for both datasets. The largest source of error comes from "winter" intrusion events, and intrusions that caused negative changes in temperature. The algorithm was also used to compare the reliability between weekly and daily data acquisition in identifying intrusion events in the BBMP station. The results indicate that the weekly acquisition of data at the BBMP station was able to identify all the intrusion events present in the daily data. However, the smaller the effect caused by an intrusion event is, the higher the chances of missing

it. Moreover, in the weekly data, the algorithm was able to identify the same number of intrusion events as identified in the daily data with fewer extra intrusion events. Therefore, for intrusion identification, the weekly resolved data is preferred. Daily resolved data comes with many complexities that are avoided by using the weekly data. On the other hand, weekly data was shown to overestimate the effects of intrusion events most regularly by < 20%. So, while the weekly resolved data in the BBMP stations can identify all the intrusion events that reach the bottom, the effects from these events are most likely an overestimation.

Using the model results, 3 more stations were selected before and after the BBMP station to evaluate the continuity of the simulated intrusions. The stations are separated by the same distance and movement from ST1 to ST4 (where ST3 is the BBMP station) represents landward motion. The intrusions identified in each station were compared and continuous landward intrusions were identified. These intrusions were separated into categories based on how far along the transect they can be tracked (i.e., full, high, moderate, and low reach intrusions). The results indicate that the intrusions that make it into the Basin either make it up to ST4 or are stuck at ST1. Moreover, these intrusion events were further categorized based on the approaching speed. This is the speed at which the full extent of the effect of the intrusions were observed at ST1. Slow-approaching intrusions take longer to fully affect ST1 than it takes for the intrusion to reach ST4. Fast-approaching intrusions are intrusion events whose speed remains consistent at all stations. And finally, the muti-step intrusions are fast-approaching intrusions that get stuck in ST1 but after some time advance to ST4. It's important to note, that only because an intrusion is fast approaching does not mean that it will reach ST4, and only because and intrusion is slow approaching, it does not mean it won't reach ST4. Earlier in the year slow-approaching intrusion events are predominant. The speed of the intrusion increases as the year progresses and eventually becomes fast-approaching. While there are not many intrusion events affecting the bottom of the Basin from July to September, the model simulation shows that there might be a lot of fast-approaching intrusion only making it to ST1. This indicates that while the BBMP station can record all the intrusion events that make it to the bottom of the Basin, it cannot record the intrusions that remain at ST1.

CHAPTER 4

SUMMARY AND DISCUSSION

Lateral intrusions of water masses from the Scotian Shelf are a common occurrence in Bedford Basin. These intrusion events bring water masses that are relatively warmer, saltier, more oxygenated, and more nitrate-depleted than the preexisting water in the Basin. The interaction between bottom waters and the intrusion event is known to prevent the development of anoxic conditions at the bottom of the BB. Therefore, these intrusions act as a supply of oxygen to the Basin in between winter convection events. The BBMP dataset is a data acquisition framework located in the deepest location of BB used in this paper to characterize strong intrusion events using observational data. Most of these intrusions occur from spring to fall, but the majority of the ones observed at the BBMP dataset occur during fall. A trend observed in the data indicates that intrusion events occurring later in the year cause larger disturbances. These include larger changes in temperature, salinity, oxygen, nitrate, ammonium and their effects on water column stratification. All these factors indicate that the intrusions interacting with the BB during the fall play a larger role in deep water renewal than summer or spring intrusions.

The model used in this paper is a multi-nested model based on ROMS. This physical model is composed of 3 domains, HRM1, HRM2, and HRM3. The one-way nesting simulation of HRM2 and the two-way nesting simulation of HRM3 (i.e., HRM23) were used in this paper. The model simulations produced by HRM2 and HRM23 were used for intrusion identification and their performances were compared with the BBMP dataset and with each other. Overall, the simulations overestimate the number of intrusions in BB, especially HRM2. Similarly, both simulations also overestimate the effect on both temperature and salinity. While there are not many differences between the effects of the intrusions in the model simulations, the HRM23 captures the differences between fall and SS intrusion better than HRM2. Moreover, in terms of the effects on water column stratification, HRM2 outperforms HRM23 during fall,

but overall the simulations underestimate the homogenization of the bottom layer caused by these events. All these factors indicate that HRM23 performs better at simulating the lateral intrusion events in BB.

Since the data available from observational studies at the BBMP station are limited to weekly resolution and a single location, a model simulation of the BB (HRM23) was used to investigate how these limitations affect our understanding of these intrusion events. However, visually identifying and recording the changes caused by the intrusions in a dataset can be tedious and inconsistent. For this reason, a methodology was developed that allows for the systematic and consistent identification of strong intrusion events. Using the optimized salinity and temperature thresholds for intrusion identification, in combination with the algorithm, all the intrusions in the datasets were identified. The thresholds for HRM23 were estimated to be the same as those for the BBMP data. Similar to the observations, the majority of the errors in identification come from "winter intrusions" and intrusions causing negative changes in temperature. These thresholds and the methodology were implemented on a weekly subset of the daily data. The algorithm was able to identify the same intrusion in both datasets, however, the effects observed in the weekly data tended to be an overestimation. These results imply that the weekly resolved data can be used for intrusion identification, but to record the effects of these events daily resolved data would be preferable. The last experiments involved the categorization of intrusions based on their reach within the Basin. The categories are low (ST1), moderate (ST2), high (ST3) and full (ST4). The results indicate that the intrusions that make it into BB either get stuck in ST1 due to the presence of an underwater shelf or make it to ST4. Moreover, these intrusions can be further subdivided based on their approaching speed. The categories are slow and fast approaching, and multi-step intrusion events. These were found to be distributed through the year from slower at the start of the year and faster near the end. This is concordant with the findings from the BBMP data, where fall intrusions were observed to cause larger changes in the water column stratification of the Basin in comparison to SS intrusions. Moreover, this is also concordant with previous findings by Sui (2023), where he was able to show that natural variability in wind velocities in the area can cause SS intrusions to have a lesser impact than fall intrusions in BB.

In this thesis, intrusion events were characterized as observed from the BBMP dataset and model simulations. This information builds upon our current understanding of these events in the BB, and by comparing the simulated and observed intrusions the hope is to aid in the future development of this model. These findings show that intrusion events come in many shapes and forms and understanding these variations is critical to understand the effect of the intrusions in the Basin. Moreover, it was shown that the resolution and location of data acquisition implemented in the BBMP station are adequate for identifying these events, but for a more accurate characterization of the effects daily resolved data should be used instead. Moreover, the location of the BBMP station is adequate for identifying intrusion events reaching the bottom of the Basin. However, this station might still be missing a fair number of intrusions that do not make it to the bottom of the Basin. Future work should be focused on a more quantitative study of the effects of mixing regimes observed after and during intrusion events. This information could be helpful in the future improvement of the BB model and conversely facilitate future research in BB.

APPENDIX A

IDENTIFICATION OF CONVECTION EVENTS IN THE BEDFORD BASIN

As mentioned previously, convection events in the BB are driven by the destabilization of the water column due to decreases in surface temperatures associated with heat loss to the atmosphere. As the global trend of sea surface temperature (SST) increases at a rate of 0.007-0.012 °C/year (Hausfather et al., 2017), it could be hypothesized that the destabilization caused by the decrease in SST in winter might be weakening. Rakshit et al. (2023) studied the sources and sink of bottom water oxygen in the BB and in their analysis, they found that SST can affect the ventilation of the bottom water from both winter convection and stratified periods. They suggest that, while SST plays a role, there is a plethora of controls on water column stratification. Nevertheless, there is still potential for the hypoxia at the BB to worsen due to increasing SST. In this section, the convection events in the Basin are identified from observational data from the BBMP using the intrusion identification script from Chapter 3. Previously, the thresholds used to identify intrusion events included increases in both temperature and salinity. However, to identify convection events the thresholds were changed to oxygen and temperature. In this case, the thresholds for these variables were set to 1 mg m^{-3} $week^{-1}$ and 0.2 ºC $week^{-1}$, respectively. Unlike intrusion events, convection events can take more than a week to fully ventilate the bottom waters and the ventilation can occur in multiple steps. Therefore, from the convection events identified by the script, the complete homogenization of the water column only occurs at the last step of the convection event. Therefore, only the convection events identified last for each year were recorded. Based on this identification, ventilation of the bottom waters of the BB caused by convection has occurred yearly from 2000 to 2023, with the exception of 2006. They can occur from February to April. Figure A1 shows a few examples of this

identification. For the purpose of this thesis, the focus was on the effects of convection events on oxygen concentration in the Basin with the purpose of evaluating how this effect has changed from 2000 – 2023.

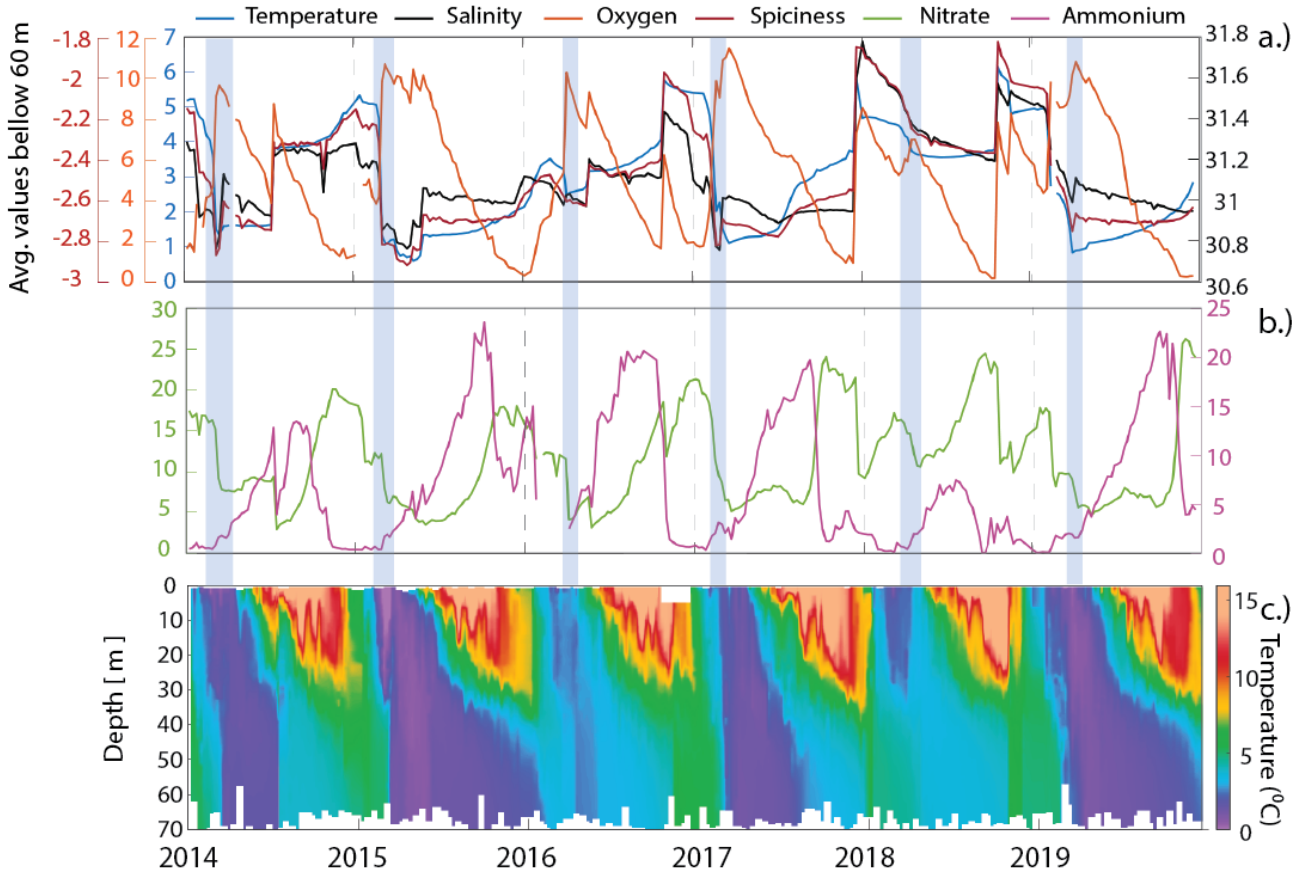

Figure A.1. a) Time-series of average temperature (ºC), salinity, oxygen (mg m^{-3}) and spiciness below 60 m at the BBMP station from 2014 - 2020. **b)** Time-series of nitrate (mmol m^{-3}) and ammonium (mmol m^{-3}) at 60 m. **c)** Time-depth distribution of temperature. The tick marks and the dashed lines in the x-axis mark January 1 of each year. These figures were used to identify convection events (blue) in the BBMP data.

Figure A2 shows every convection event identified within the time period and the corresponding oxygen concentrations observed in the Basin after each event. This figure does not show a decreasing trend in oxygen concentration observed after convection events. However, after the convection events in 2021, there is a record of the lowest oxygen concentrations observed at the bottom of the Basin. To put this into perspective, the average concentration of oxygen observed in bottom waters after the events was 9.50 ±

1.81 mg m^{-3} (excluding 2021), and in 2021 the oxygen concentration was 3.80 mg m^{-3}. Similar to the findings from Rakshit et al. (2023), my findings imply that there is no decreasing trend in ventilation from convection events. However, the occurrence of the 2021 convection event might indicate that the stress being inflicted by global warming might be starting to significantly affect the reliability of these events at ventilating the bottom waters of the BB.

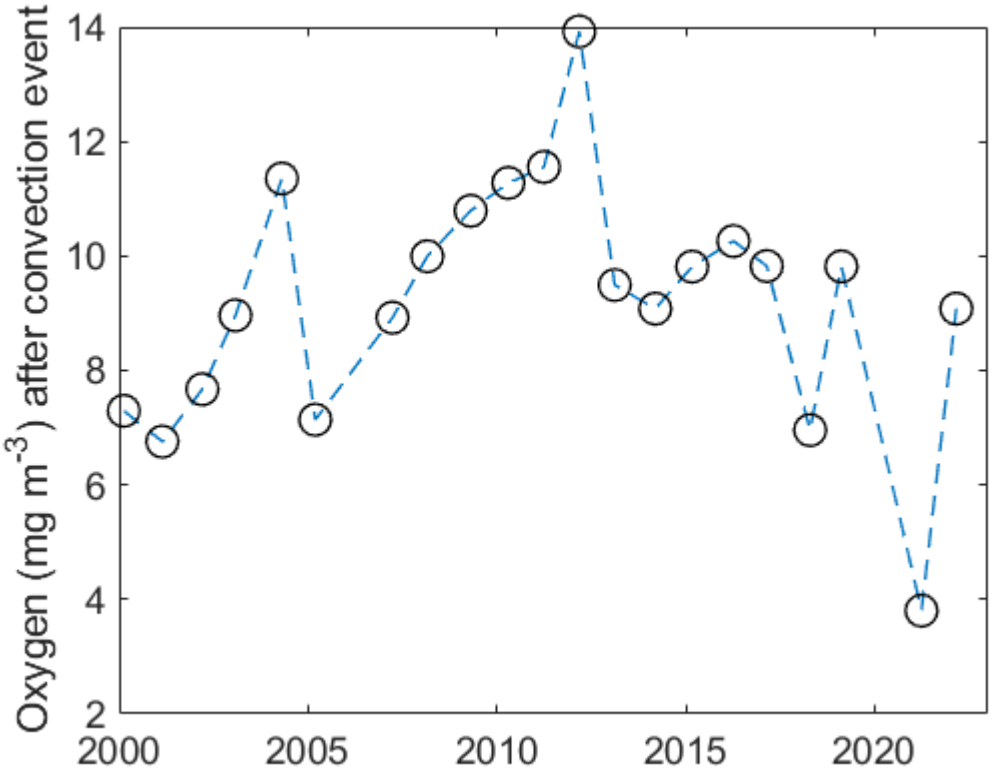

Figure A.2. Time-series of oxygen concentrations (mg m^{-3}) observed after each convection event identified below 60 m at the BBMP station from 2000 – 2023. No convection events were observed in 2006, while 2020 was omitted due to a lack of sufficient data.

APPENDIX B

SUPPLEMENTARY FIGURES

Strong lateral intrusion identification was carried out in the model results from 2003 to 2023 (Figures B1 and B2). The same identification was carried out for the entire BBMP dataset which spans from 1999 to 2023 (Figures B3, B4, B5, and B6). In addition, the post-intrusion conditions were recorded and a time series of each variable was created to observe the changes in the disturbance caused by the intrusion event from 2000 – 2023. This includes temperature (B7), salinity (B8), nitrate (B9), ammonium (B10), and oxygen (B11). These figures do not show any trends. However, the post-intrusion temperature and salinity conditions at depth have been increasing since 2015. On the other hand, the post-intrusion oxygen concentrations at depth have been decreasing since 2015. These are not the lowest oxygen concentrations recorded after an intrusion event, however, these are the most consistent relatively low concentrations of oxygen recorded at depth since 1999. However, it is also important to note that no information is available for 2020.

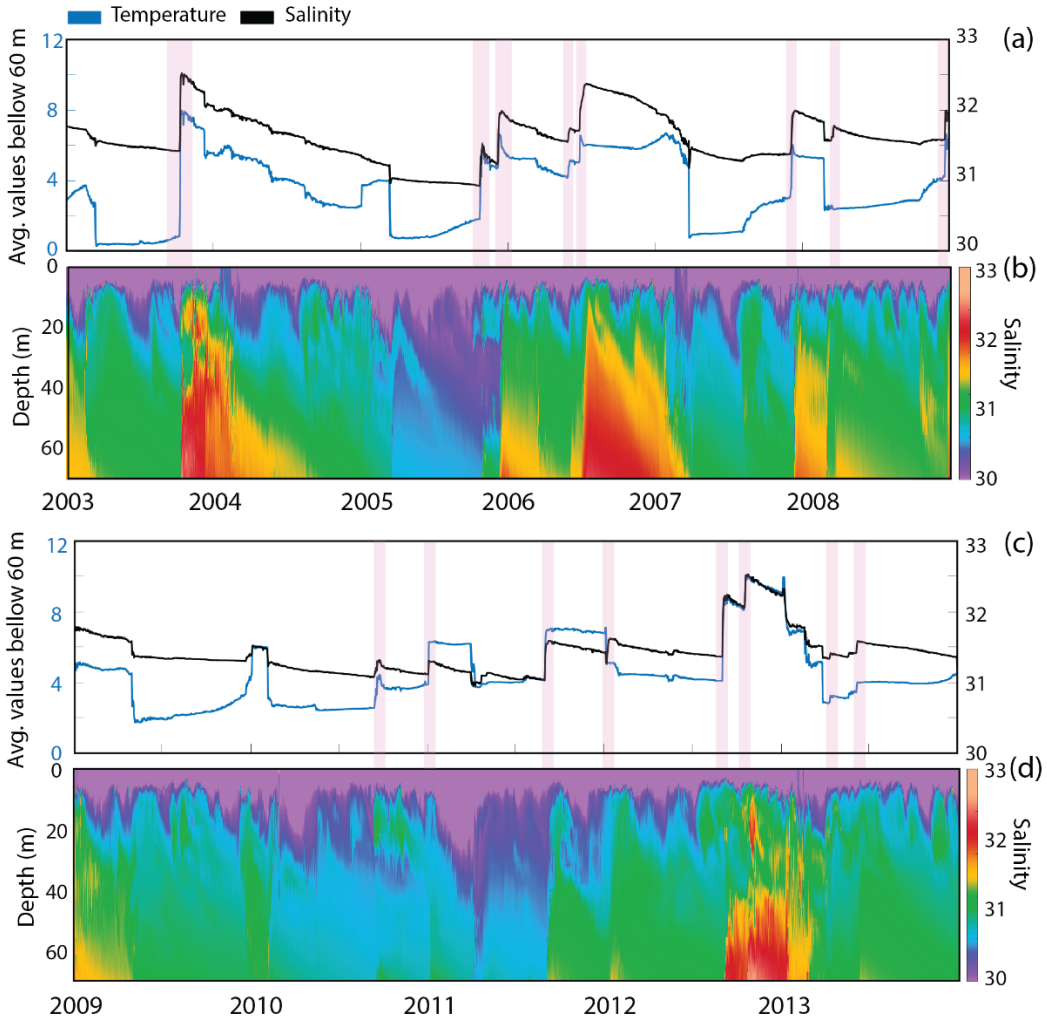

Figure B.1. Time-series of average temperature (ºC), and salinity below 60 m at the BBMP station from 2003 – 2013, from model simulation. And time-depth distribution of salinity. The tick marks and the dashed lines in the x-axis mark January 1 of each year. These figures were used to identify intrusion events (pink) in the model simulation HRM23.

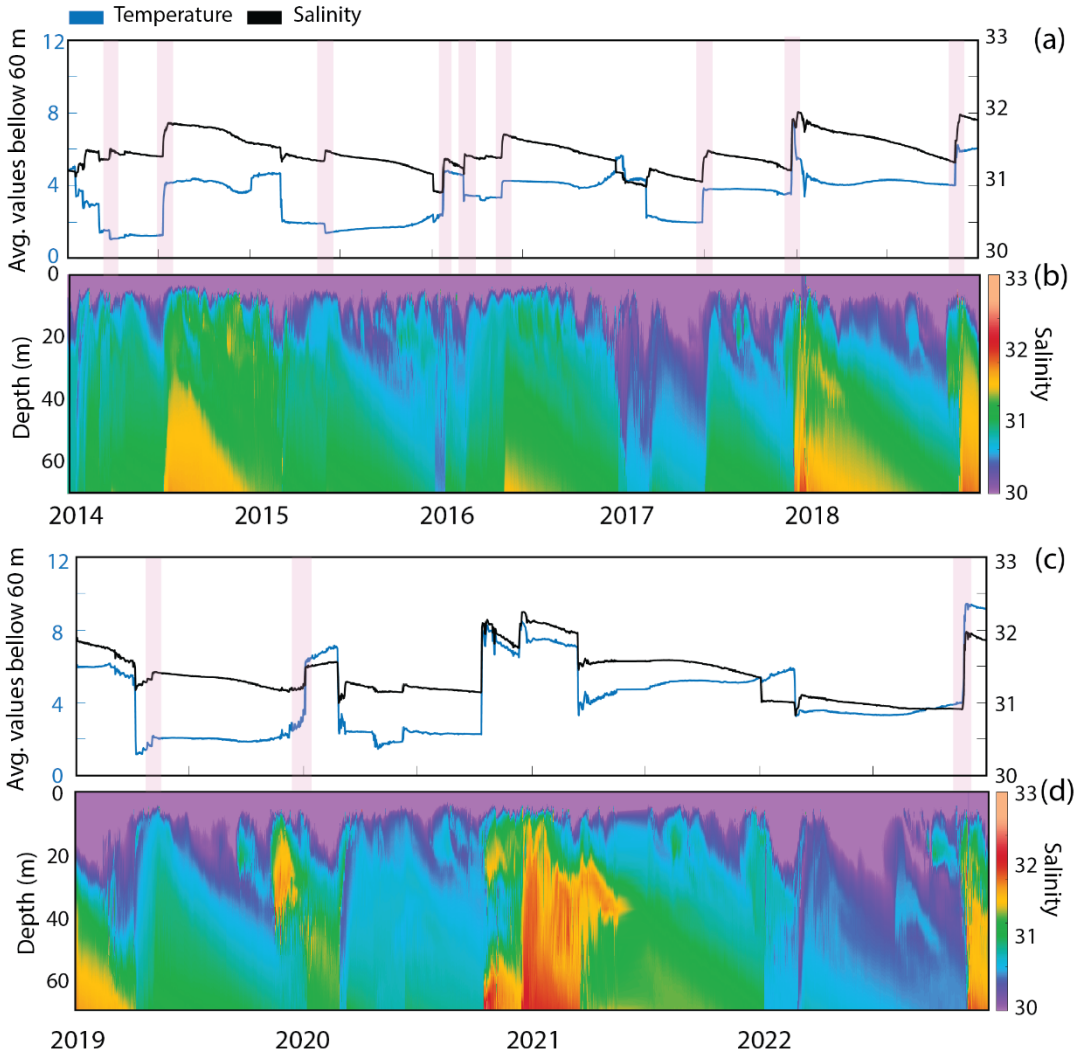

Figure B.2. Time-series of average temperature (ºC), and salinity below 60 m at the BBMP station from 2014 – 2023, from model simulation. And time-depth distribution of salinity. The tick marks and the dashed lines in the x-axis mark January 1 of each year. These figures were used to identify intrusion events (pink) in the model simulation HRM23.

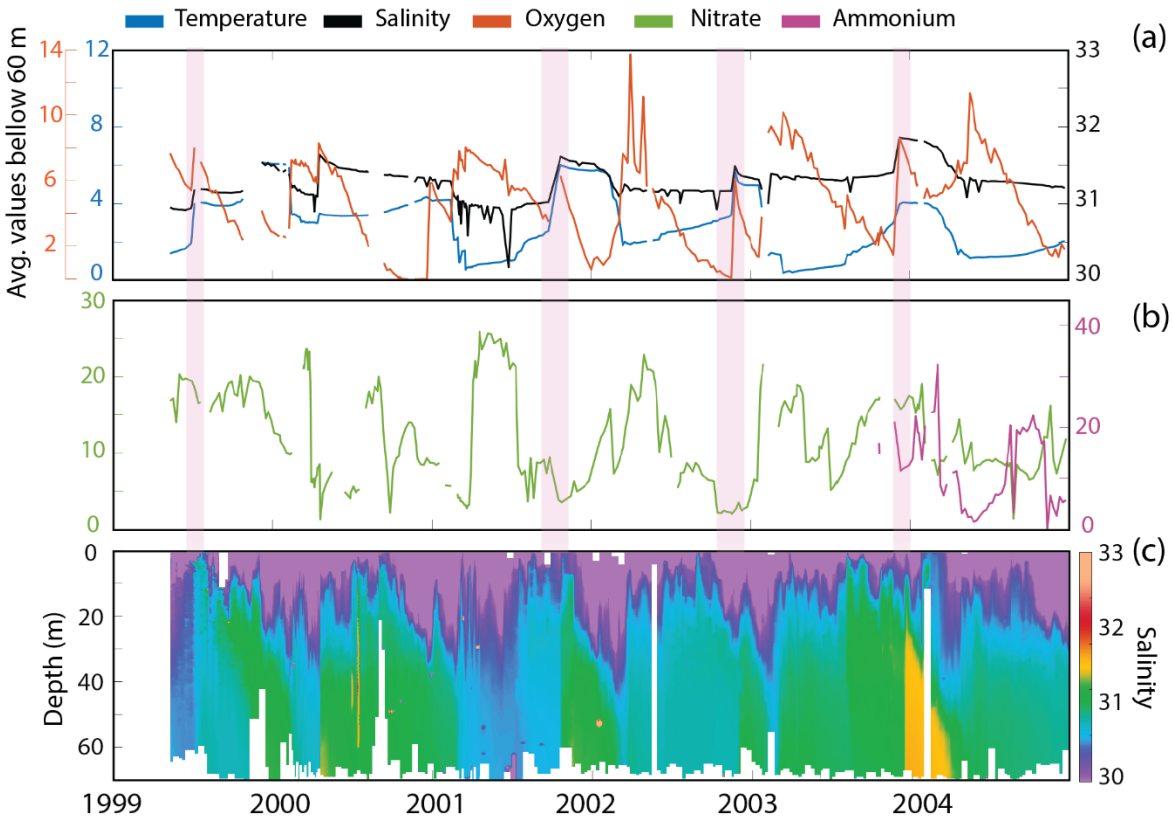

Figure B.3. Time series of average temperature (ºC), salinity, and oxygen (mg m^{-3}) below 60 m at the BBMP station from 1999 - 2005. Time-series of nitrate (mmol m^{-3}) and ammonium (mmol m^{-3}) at 60 m. And time-depth distribution of salinity. The tick marks and the dashed lines in the x-axis mark January 1 of each year. These figures were used to identify intrusion events (pink) in the BBMP data.

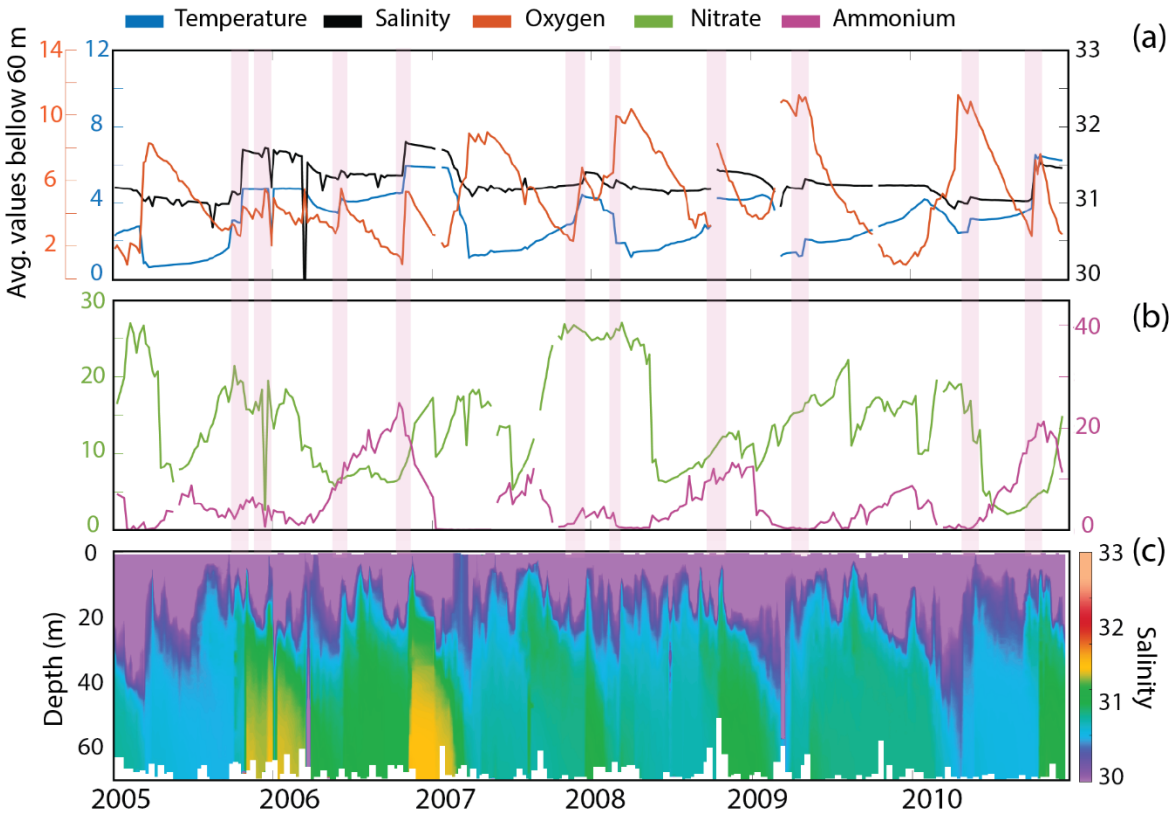

Figure B.4. Time series of average temperature (ºC), salinity, and oxygen (mg m^{-3}) below 60 m at the BBMP station from 2005 - 2011. Time-series of nitrate (mmol m^{-3}) and ammonium (mmol m^{-3}) at 60 m. And time-depth distribution of salinity. The tick marks and the dashed lines in the x-axis mark January 1 of each year. These figures were used to identify intrusion events (pink) in the BBMP data.

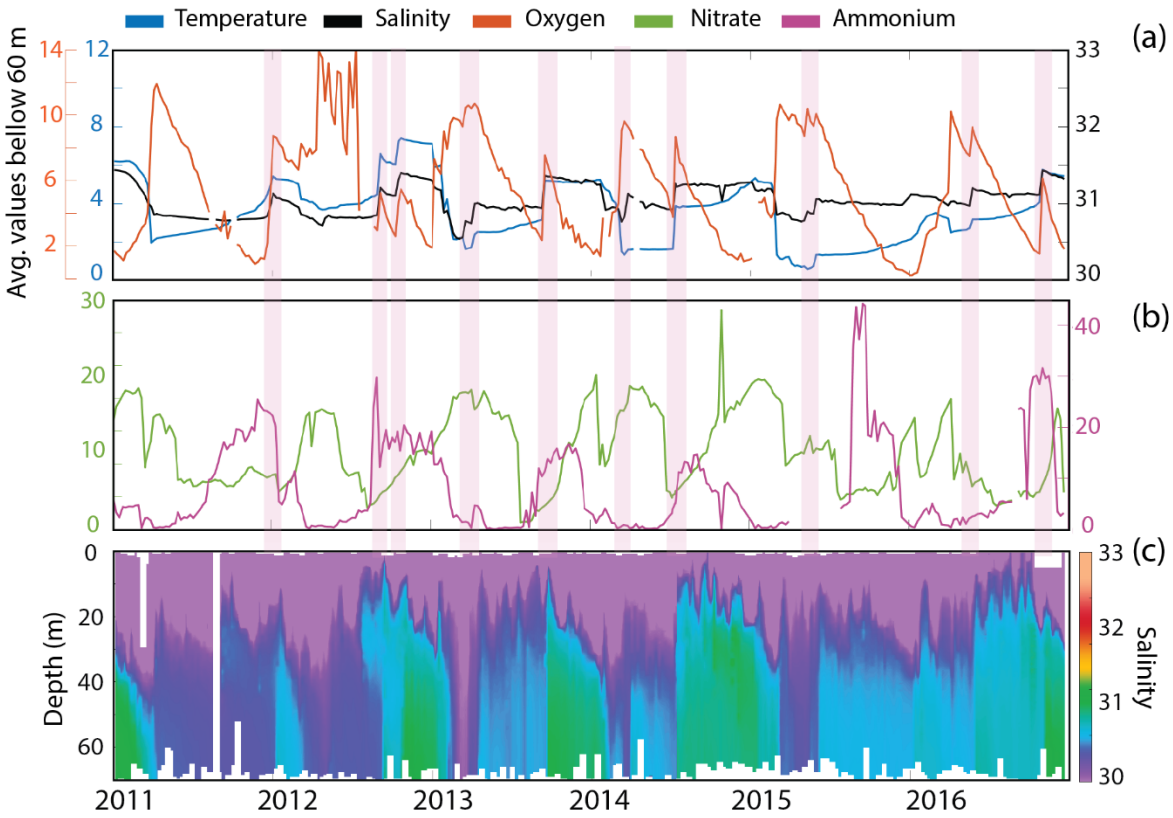

Figure B.5. Time series of average temperature (ºC), salinity, and oxygen (mg m^{-3}) below 60 m at the BBMP station from 2011 - 2017. Time-series of nitrate (mmol m^{-3}) and ammonium (mmol m^{-3}) at 60 m. And time-depth distribution of salinity. The tick marks and the dashed lines in the x-axis mark January 1 of each year. These figures were used to identify intrusion events (pink) in the BBMP data.

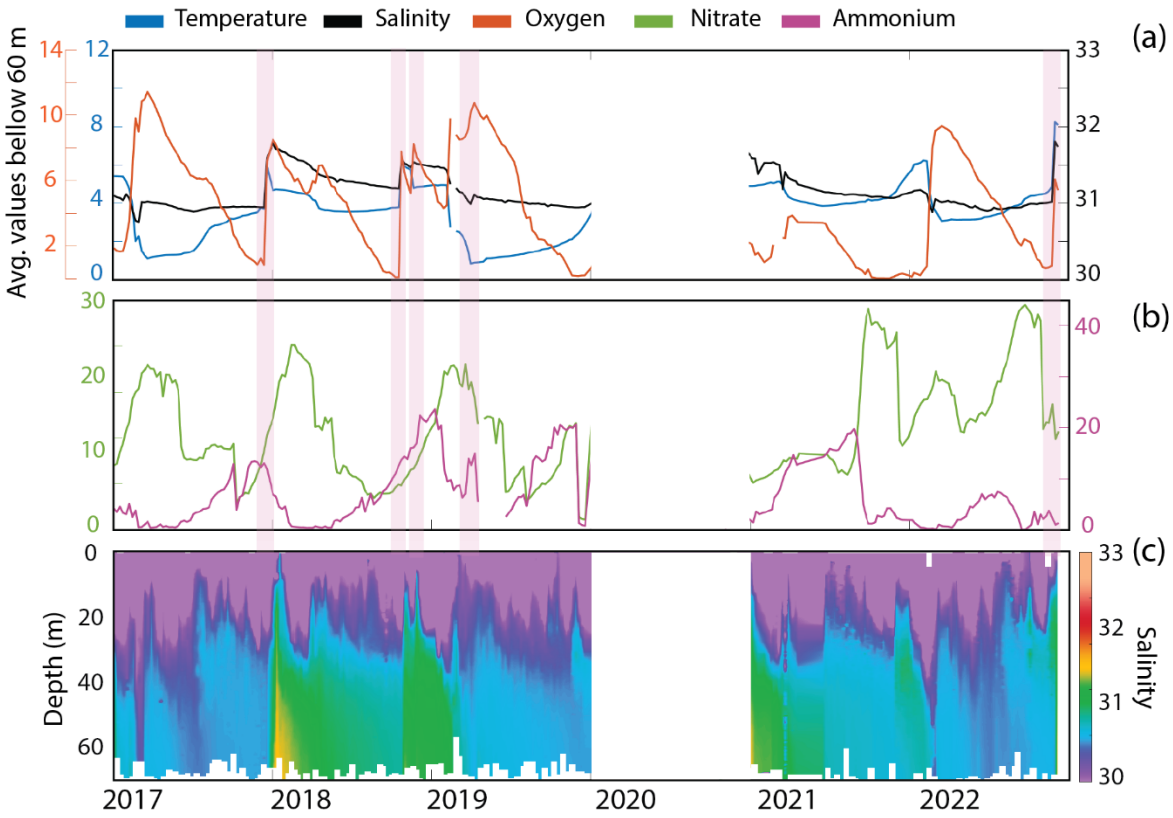

Figure B.6. Time series of average temperature (ºC), salinity, and oxygen (mg m^{-3}) below 60 m at the BBMP station from 2017 - 2023. Time-series of nitrate (mmol m^{-3}) and ammonium (mmol m^{-3}) at 60 m. And time-depth distribution of salinity. The tick marks and the dashed lines in the x-axis mark January 1 of each year. These figures were used to identify intrusion events (pink) in the BBMP data.

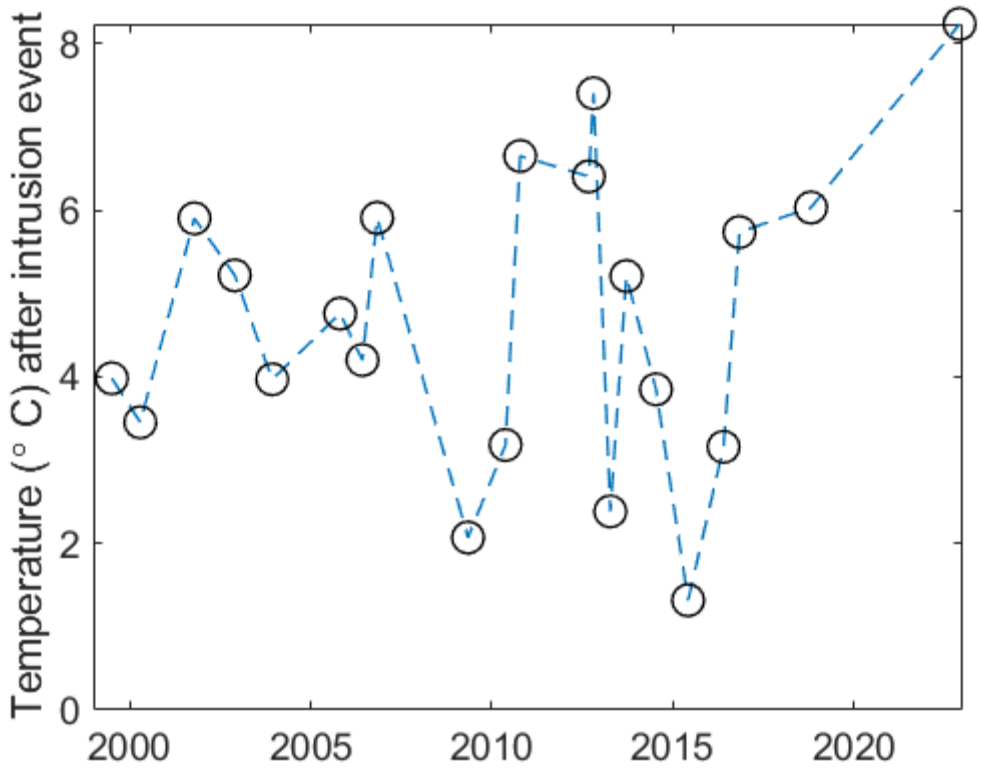

Figure B.7. Time-series of temperatures observed after each strong intrusion event identified below 60 m at the BBMP station from 2000 – 2023.

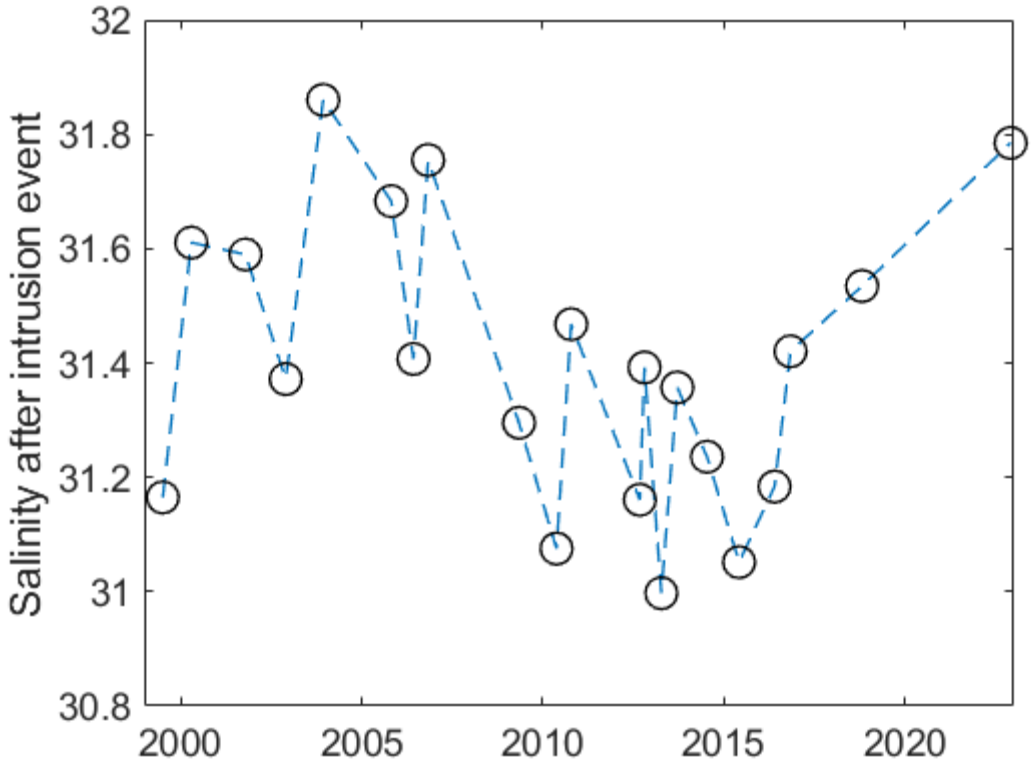

Figure B.8. Time-series of salinity observed after each strong intrusion event identified below 60 m at the BBMP station from 2000 – 2023.

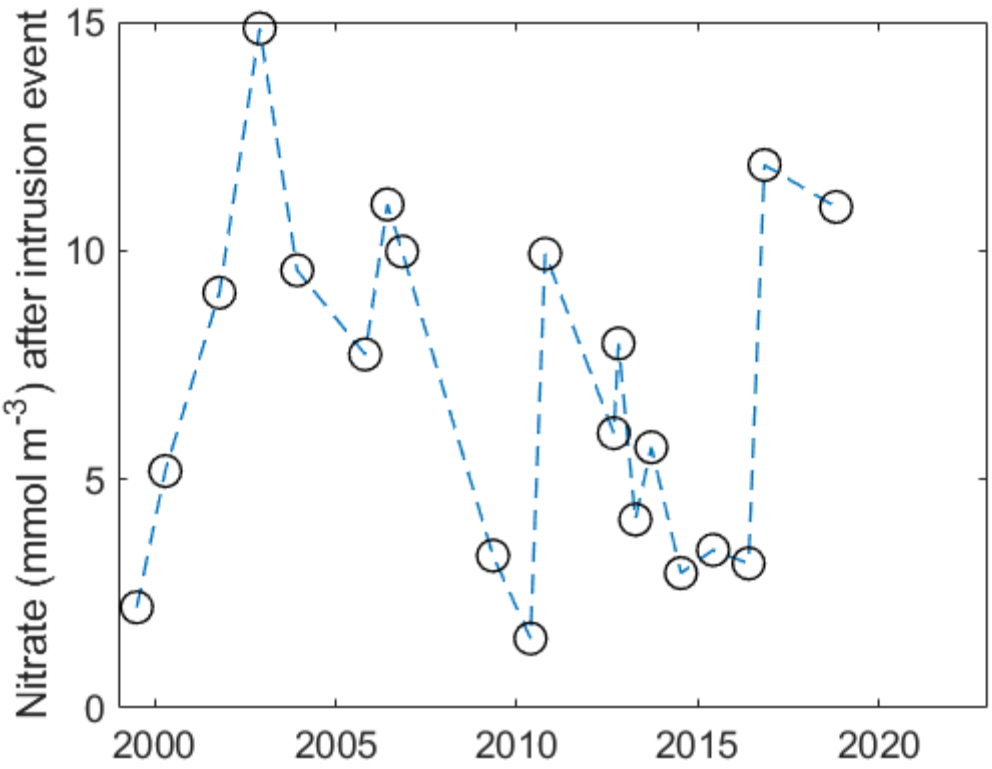

Figure B.9. Time-series of nitrate concentrations observed after each strong intrusion event identified below 60 m at the BBMP station from 2000 – 2023.

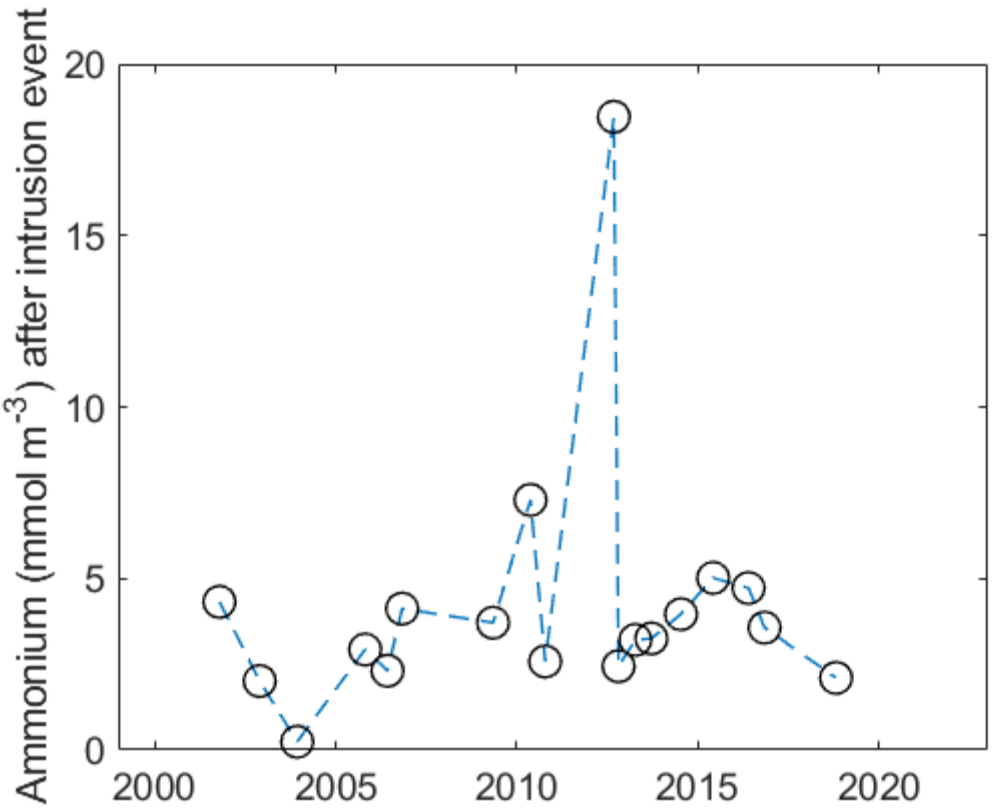

Figure B.10. Time-series of ammonium concentrations observed after each strong intrusion event identified below 60 m at the BBMP station from 2000 – 2023.

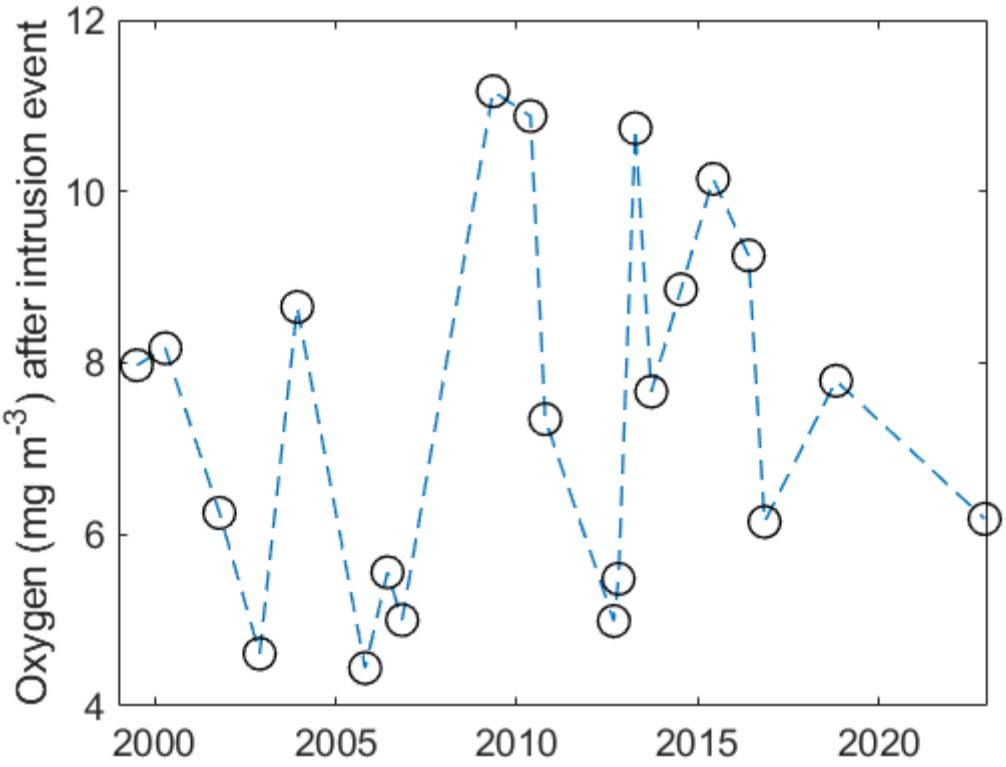

Figure B.11. Time-series of oxygen concentrations observed after each strong intrusion event identified below 60 m at the BBMP station from 2000 – 2023.

BIBLIOGRAPHY

Azetsu-Scott, K., & Johnson, B. D. (1994). Time series of the vertical distribution of particles during and after a spring phytoplankton bloom in a coastal basin. *Continental Shelf Research*, *14*(6), 687–705. https://doi.org/10.1016/0278-4343(94)90113-9

Brennan, C. E., Bianucci, L., & Fennel, K. (2016). Sensitivity of Northwest North Atlantic Shelf Circulation to Surface and Boundary Forcing: A Regional Model Assessment. *Atmosphere-Ocean*, *54*(3), 230–247. https://doi.org/10.1080/07055900.2016.1147416

Buckley, D. E., & Winters, G. V. (1992). Geochemical characteristics of contaminated surficial sediments in Halifax Harbour: Impact of waste discharge. *Canadian Journal of Earth Sciences*, *29*(12), 2617–2639. https://doi.org/10.1139/e92-208

Burt, W. J., Thomas, H., Fennel, K., & Horne, E. (2013). Sediment-water column fluxes of carbon, oxygen and nutrients in Bedford Basin, Nova Scotia, inferred from 224Ra measurements. *Biogeosciences*, *10*(1), 53–66. https://doi.org/10.5194/bg-10-53-2013

Fader, G. B., & Miller, R. O. (2008). *Surficial geology, Halifax Harbour, Nova Scotia*. Natural Resources Canada.

Fennel, K., Hetland, R., Feng, Y., & DiMarco, S. (2011). A coupled physical-biological model of the Northern Gulf of Mexico shelf: Model description, validation and analysis of phytoplankton variability. *Biogeosciences*, *8*(7), 1881–1899. https://doi.org/10.5194/bg-8-1881-2011

Fennel, K., & Testa, J. M. (2019). Biogeochemical Controls on Coastal Hypoxia. *Annual Review of Marine Science*, *11*(1), 105–130. https://doi.org/10.1146/annurev-marine-010318-095138

Fennel, K., Wilkin, J., Levin, J., Moisan, J., O'Reilly, J., & Haidvogel, D. (2006). Nitrogen cycling in the Middle Atlantic Bight: Results from a three-dimensional model and implications for the North Atlantic nitrogen budget: NITROGEN CYCLING IN THE MIDDLE ATLANTIC. *Global Biogeochemical Cycles*, *20*(3), n/a-n/a. https://doi.org/10.1029/2005GB002456

Fennel, K., Wilkin, J., Previdi, M., & Najjar, R. (2008). Denitrification effects on air-sea CO_2 flux in the coastal ocean: Simulations for the northwest North Atlantic. *Geophysical Research Letters*, *35*(24), L24608. https://doi.org/10.1029/2008GL036147

Flament, P. (2002). A state variable for characterizing water masses and their diffusive stability: Spiciness. *Progress in Oceanography*, *54*(1–4), 493–501. https://doi.org/10.1016/S0079-6611(02)00065-4

Fournier, R. (1990). *Final Report of the Halifax Harbour Task Force*. http://legacycontent.halifax.ca/harboursol/documents/FournierHalifaxHarbourTaskForceFinalReport1990.pdf

Greenberg, D. A. (1999). Atlas of Tidal Currents for Halifax Harbour, http://www.mar.dfo-mpo.gc.ca/science/ocean/coastal hydrodynamics/atlas/atlas.pdf

Gregory, D., Petrie, B., Jordan, F., & Langile, P. (1993). Oceanographic, geographic, and hydrological parameters of Scotia-Fundy and Suthern Gulf of ST. Lawrence inlets. *Can. Tech. Rep. Hydrogr. Ocean Sci.*, *.No. 143*, viii+248pp.

Haas, S., Rakshit, S., Kalvelage, T., Buchwald, C., Algar, C. K., & Wallace, D. W. R. (2022). Characterization of nitrogen isotope fractionation during nitrification based on a coastal time series. *Limnology and Oceanography*, *67*(8), 1714–1731. https://doi.org/10.1002/lno.12161

Haas, S., Robicheau, B. M., Rakshit, S., Tolman, J., Algar, C. K., LaRoche, J., & Wallace, D. W. R. (2021). Physical mixing in coastal waters controls and decouples nitrification via biomass dilution. *Proceedings of the National Academy of Sciences*, *118*(18), e2004877118. https://doi.org/10.1073/pnas.2004877118

Haidvogel, D. B., Arango, H., Budgell, W. P., Cornuelle, B. D., Curchitser, E., Di Lorenzo, E., Fennel, K., Geyer, W. R., Hermann, A. J., Lanerolle, L., Levin, J., McWilliams, J. C., Miller, A. J., Moore, A. M., Powell, T. M., Shchepetkin, A. F., Sherwood, C. R., Signell, R. P., Warner, J. C., & Wilkin, J. (2008). Ocean forecasting in terrain-following coordinates: Formulation and skill assessment of the Regional Ocean Modeling System. *Journal of Computational Physics*, *227*(7), 3595–3624. https://doi.org/10.1016/j.jcp.2007.06.016

Hargrave, B. T., Phillips, G. A., & Taguchi, S. (1976). Sedimentation measurements in Bedford Basin, 1973-74. *Tech. Rep. Fish. Mar. Serv. Envir.*, *608*, 1–129. https://doi.org/10.13140/2.1.2815.3125

Hausfather, Z., Cowtan, K., Clarke, D. C., Jacobs, P., Richardson, M., & Rohde, R. (2017). Assessing recent warming using instrumentally homogeneous sea surface temperature records. *Science Advances*, *3*(1), e1601207. https://doi.org/10.1126/sciadv.1601207

Huntsman, A. G. (1924). Circulation and pollution of water in adn near Halifax Harbour. *Contributions to Canadian Biology and Fisheries*, *2*(1), 69–80. https://doi.org/10.1139/f24-003

Kerrigan, E. A., Kienast, M., Thomas, H., & Wallace, D. W. R. (2017). Using oxygen isotopes to establish freshwater sources in Bedford Basin, Nova Scotia, a Northwestern Atlantic fjord. *Estuarine, Coastal and Shelf Science*, *199*, 96–104. https://doi.org/10.1016/j.ecss.2017.09.003

La Roche, J. (1983). Ammonium regeneration: Its contribution to phytoplankton nitrogen requirements in a eutrophic environment. *Marine Biology*, *75*(2–3), 231–240. https://doi.org/10.1007/BF00406007

Lacasse, O., Rochon, A., & Roy, S. (2013). High cyst concentrations of the potentially toxic dinoflagellate Alexandrium tamarense species complex in Bedford Basin, Halifax, Nova Scotia, Canada. *Marine Pollution Bulletin*, *66*(1–2), 230–233. https://doi.org/10.1016/j.marpolbul.2012.10.016

Laurent, A., Fennel, K., & Kuhn, A. (2021). An observation-based evaluation and ranking of historical Earth system model simulations in the northwest North Atlantic Ocean. *Biogeosciences*, *18*(5), 1803–1822. https://doi.org/10.5194/bg-18-1803-2021

Laurent, A., Fennel, K., Wilson, R., Lehrter, J., & Devereux, R. (2016). Parameterization of biogeochemical sediment–water fluxes using in situ measurements and a diagenetic model. *Biogeosciences*, *13*(1), 77–94. https://doi.org/10.5194/bg-13-77-2016

Li, W. K. W., & Glen Harrison, W. (2008). Propagation of an atmospheric climate signal to phytoplankton in a small marine basin. *Limnology and Oceanography*, *53*(5), 1734–1745. https://doi.org/10.4319/lo.2008.53.5.1734

Li, W. K. W., Lewis, M. R., & Harrison, W. G. (2010). Multiscalarity of the Nutrient–Chlorophyll Relationship in Coastal Phytoplankton. *Estuaries and Coasts*, *33*(2), 440–447. https://doi.org/10.1007/s12237-008-9119-7

McGonigal, D., Loucks, R., & Ingraham, D. (1974). Halifax narrows: Sample current meter data 1970-71. *BIO Data Series BI-D74-5*.

Miller, A. A. L., Mudie, P. J., & Scott, D. B. (1982). Holocene history of Bedford Basin, Nova Scotia: Foraminifera, dinoflagellate, and pollen records. *Canadian Journal of Earth Sciences*, *19*(12), 2342–2367. https://doi.org/10.1139/e82-205

Pan, Y., & Subba Rao, D. V. (1997). Impacts of domestic sewage effluent on phytoplankton from Bedford Basin, eastern Canada. *Marine Pollution Bulletin*, *34*(12), 1001–1005. https://doi.org/10.1016/S0025-326X(97)00115-X

Petrie, B., & Yeats, P. (1990). Simple Models of the Circulation, Dissolved Metals, Suspended Solids and Nutrients in Halifax Harbour. *Water Quality Research Journal*, *25*(3), 325–350. https://doi.org/10.2166/wqrj.1990.017

Platt, T. (1975). Analysis of the importance of spatial and temporal heterogeneity in the estimation of annual production by phytoplankton in a small, enriched, marine basin. *Journal of Experimental Marine Biology and Ecology*, *18*(2), 99–109. https://doi.org/10.1016/0022-0981(75)90067-2

Platt, T., & Conover, R. J. (1971). Variability and its effect on the 24h chlorophyll budget of a small marine basin. *Marine Biology*, *10*(1), 52–65. https://doi.org/10.1007/BF02026766

Platt, T., Prakash, A., & Irwin, B. (1972). Phytoplankton nutrients and flushing of inlets on the coast of Nova Scotia, Nat. Can., 99, 253261, 1972. *Nat. Can.*, *99*, 253–261.

Punshon, S., & Moore, R. M. (2004). Nitrous oxide production and consumption in a eutrophic coastal embayment. *Marine Chemistry*, *91*(1–4), 37–51. https://doi.org/10.1016/j.marchem.2004.04.003

Rabouille, C., Lansard, B., Owings, S. M., Rabalais, N. N., Bombled, B., Metzger, E., Richirt, J., Eitel, E. M., Boever, A. D., Beckler, J. S., & Taillefert, M. (2021). Early Diagenesis in the Hypoxic and Acidified Zone of the Northern Gulf of Mexico: Is Organic Matter Recycling in Sediments Disconnected From the Water Column? *Frontiers in Marine Science*, *8*, 604330. https://doi.org/10.3389/fmars.2021.604330

Rakshit, S., Dale, A. W., Wallace, D. W., & Algar, C. K. (2023). Sources and sinks of bottom water oxygen in a seasonally hypoxic fjord. *Frontiers in Marine Science*, *10*, 1148091. https://doi.org/10.3389/fmars.2023.1148091

Rutherford, K., Fennel, K., Atamanchuk, D., Wallace, D., & Thomas, H. (2021). A modelling study of temporal and spatial CO variability on the biologically active and temperature-dominated Scotian Shelf. *Biogeosciences*, *18*(23), 6271–6286. https://doi.org/10.5194/bg-18-6271-2021

Shan, S. (2010). Numerical Study of Three-dimensional Circulation and Hydrography in Halifax Harbour Using a Nested-grid Ocean Circulation Model (Master's Thesis). Retrieved from DalSpace Institutional Repository. (URI: http://hdl.handle.net/10222/13173)

Shan, S., Sheng, J., Thompson, K. R., & Greenberg, D. A. (2011). Simulating the three-dimensional circulation and hydrography of Halifax Harbour using a multi-nested coastal ocean circulation model. *Ocean Dynamics*, *61*(7), 951–976. https://doi.org/10.1007/s10236-011-0398-3

Shi, Q., & Wallace, D. (2018). A 3-year time series of volatile organic iodocarbons in Bedford Basin, Nova Scotia: A northwestern Atlantic fjord. *Ocean Science*, *14*(6), 1385–1403. https://doi.org/10.5194/os-14-1385-2018

Sui, Y. (2023). Study of temperature, salinity, and circulation over coastal and shelf waters using nested-grid circulation models (Doctoral dissertation). Retrieved from DalSpace Institutional Repository. (URI: http://hdl.handle.net/10222/82584)

Tee, K. T., & Petrie, B. (1991). A two-dimensional baroclinic model for the Halifax Harbour. In Proceedings second Halifax inlet research workshop. Dartmouth, NS.

Therriault, J.-C., Petrie, B., Pepin, P., Gagnon, J., Gregory, D., Helbig, J., Herman, A., Lefaivre, D., Mitchel, M., Pelchat, B., Runge, J., and Sameoto, D. (1998). Proposal for a Northwest Atlantic Zonal Monitoring Program. Can. Tech. Rep. Hydro. and Ocean Sci. 194, vii + 57 p.